Available online at www.sciencedirect.com
SCIENCE DIRECT®
Computers and Structures 84 (2006) 624–639
Computers & Structures
www.elsevier.com/locate/compstruc

A mixed FSDT finite element for monoclinic laminated plates

Ferdinando Auricchio [a], Elio Sacco [b], Giuseppe Vairo [c,*]

[a] Dip. Meccanica Strutturale, Università di Pavia, 27100, Italy
[b] Dip. Meccanica, Strutture, A. & T., Università di Cassino, 03043, Italy
[c] Dip. Ingegneria Civile, Università di Roma "Tor Vergata", Via del Politecnico 1, 00133 Rome, Italy

Received 5 November 2004; accepted 10 October 2005
Available online 19 January 2006

Abstract

A 4-node finite element for the analysis of laminated composite plates with monoclinic layers, as it occurs for example in piezoelectric applications, is developed. The element is built through the linked interpolation scheme proposed by Taylor and Auricchio [Int J Numer Meth Eng 1993;36:3057–66] and is a generalization of the element presented in [Auricchio F, Sacco E. A mixed-enhanced finite-element for the analysis of laminated composite plates. Int J Numer Meth Eng 1999;44:1481–1504]. Starting from a first-order shear deformation theory (FSDT), a mixed-enhanced variational formulation is considered. It includes as primary variables the resultant shear stresses as well as enhanced incompatible modes, which are introduced to improve in-plane deformations. Bubble functions for rotation degrees of freedom and functions linking transversal displacement to rotations are employed. The solvability of the variational formulation is proved whereas effectiveness and convergence of the proposed finite element are confirmed through several numerical applications. Finally, numerical results are compared with the corresponding analytical solutions as well as to other finite-element solutions.
© 2005 Elsevier Ltd. All rights reserved.

Keywords: Composite laminated plates; First-order shear deformation theory (FSDT); Monoclinic constitutive symmetry; Mixed-enhanced finite-element formulation

1. Introduction

The wide development of laminated composite plates and their large use in a variety of complex structures, especially in space, automotive and civil applications, may be clearly related to the improvement in performance-to-weight ratios in comparison with the homogeneous case.

Owing to their anisotropic response the behaviour of laminated plates generally involves extension-bending coupling. Furthermore, they are usually characterized by small values of shear moduli along the thickness direction in comparison with the longitudinal in-plane ones. As a consequence, non-negligible shear deformations in the thickness are often induced.

On the other hand, determining in an accurate way the interlaminar transversal stresses (i.e. shear stresses at the interface between two adjacent laminae) represents a very important engineering task because they are responsible for activation and development of delamination process.

Nowadays many commercial finite-element codes contain laminated-plate and -shell elements. Nevertheless, modelling and analysing laminated composite plates, because of their complex behaviour, can be still considered actual scientific issues.

Owing to geometrical considerations, concerning the small dimensions of the thickness in comparison with the in-plane ones, laminated plates are usually analysed through two-dimensional models. These latter are generally obtained from the 3D theories assuming a specific structural behaviour, that is introducing opportune assumptions on the strain field or on the stress one, or on both of them. Accordingly, several laminate plate theories as well as many refinements of classical models have been proposed in the

* Corresponding author. Tel.: +39 06 72597088; fax: +39 06 72597005.
E-mail address: vairo@ing.uniroma2.it (G. Vairo).

0045-7949/$ - see front matter © 2005 Elsevier Ltd. All rights reserved.
doi:10.1016/j.compstruc.2005.10.008

recent specialistic literature (e.g. [1,4,22,24,26,34,39]). Two different approaches may be distinguished and they lead to distinct classes of laminate theories: equivalent single layer theories (ESLTs) and layer wise theories (LWTs) [19].

ESLTs represent the direct extension of plate theories to the case of laminated plates and their main features concern the use of global assumptions on strain or stress fields in the whole thickness of the laminate. Accordingly, the laminate is reduced to a single-layer plate with an equivalent anisotropic response.

On the contrary, LWTs are obtained introducing hypotheses on the behaviour of each lamina (e.g. [13]). As a consequence, while for ESLTs the number of displacement variables does not depend on the number of layers, for LWTs the same variables are independent in each layer. Accordingly, models which arise from LWTs are generally expensive from a computational point of view.

A simple equivalent single-layer theory is the classical laminate plate theory (CLPT) (e.g. [34]). It represents an extension of the Kirchhoff–Love plate theory and it does not take into account shear deformations. As a consequence, the approximation could be quite poor. Furthermore, in the framework of finite element procedures (cf. [11,23]), CLPT models require C^1-conforming schemes, which are quite expensive from a computational point of view.

Models arising from the Reissner–Mindlin plate theory [29,35] (indicated in the following as first-order shear deformation theory: FSDT) are often preferred. This approach, which was originally developed by Yang et al. [41] and by Whitney and Pagano [40], allows us to take into account shear deformation effects in a simple way. Accordingly, accurate solutions can be obtained even for moderately thick laminates. Moreover, from a computational point of view, C^0-conforming methods can be employed. It is worth observing that the correct use of the FSDT generally requires the introduction of *shear correction factors*. They are defined through the exact profiles of the shear stresses and they have a great influence on the overall structural response. Unfortunately, they are known a priori only for homogeneous plates or for simple problems (e.g. [25]) whereas closed-form expressions are not available for general cases. Therefore, this aspect represents a clear FSDT's limitation. In order to overcome this difficulty, several approaches can be found in literature: refinement of the model by using additive shear warping functions (e.g. [32]); use of iterative procedures based on explicit analytical solutions (e.g. [30]) or on numerical solutions (e.g. [5]); refinement of the model in order to avoid using shear correction factors (e.g. [4,8]).

The literature confirms (e.g. [18,24]) that FSDT gives the best compromise between prediction ability and computational costs for a wide class of laminate problems. Four-node elements are often preferred with respect to the 8- or 9-node ones because they allow simpler discretization procedures as well as easier extensions to the finite deformation regime. On the other hand, 4-node displacement-based elements adopt simple interpolation functions which do not produce a satisfactory recovery for the through-the-thickness shear stresses. Accordingly, although the most common FSDT variational formulations are based on displacement approaches, hybrid and partially hybrid stress formulations have been proposed in recent works (e.g. [4,21,33]).

Moreover, laminated-plate elements which are contained in many commercial finite-element codes and which are usually proposed in literature are formulated considering layers having at least an orthotropic constitutive symmetry. On the other hand, in general cases, such as piezoelectric applications, the laminate problem can be properly described only if monoclinic layers are considered.

This work starts with a review of the 3D laminated-plate problem together with a detailed discussion of the basic hypotheses which are introduced to build the 2D model within a FSDT approach. Techniques usually adopted for the recovery of transversal shear stresses are also presented. Hence, starting from the Hu–Washizu functional specialized to the case of a 3D laminate, a two-dimensional mixed-enhanced variational formulation is deduced. The existence and uniqueness of the continuous solution is discussed and, generalizing the formulation proposed by Auricchio and Sacco in [5], a 4-node finite element for laminated composite plates formed by monoclinic layers is developed. The element uses enhanced incompatible modes to improve the in-plane deformations, bubble functions for the rotation degrees of freedom and functions which link the transversal displacement to the rotations. It is able to provide accurate in-plane/out-of-plane deformations, as well as accurate shear and normal stress profiles. Moreover, as theoretically expected and as proved through several numerical tests, the element exhibits a h convergence rate in H^1 energy-type norm and it does not suffer from zero energy modes.

2. Laminated-plate problem and FSDT model

The term laminated plate refers to a 3D flat body Ω, defined as:

$$\Omega = \left\{(x_1, x_2, z) \in \mathbb{R}^3 : z \in (-t/2, t/2),\ (x_1, x_2) \in \mathscr{P} \subset \mathbb{R}^2\right\}. \tag{1}$$

The laminate is assumed to be formed by ℓ layers perfectly bonded and whose mechanical properties can be different. The plate thickness t is assumed to be constant and the plane $z = 0$ identifies the mid-plane $\mathscr{P}$ of the undeformed plate. Top and bottom surfaces of Ω are indicated as $\mathscr{P}^+ = \mathscr{P} \times \{t/2\}$ and $\mathscr{P}^- = \mathscr{P} \times \{-t/2\}$, respectively. Moreover, the kth layer (index k assumes values in $\{1, 2, \ldots, \ell\}$) occupies the region $\mathscr{P} \times]z_{k-1}, z_k[= \Omega^{(k)}$, such that $z_0 = -t/2$ and $z_\ell = t/2$.

The boundary $\partial\mathscr{P}$ of $\mathscr{P}$ is subdivided into two complementary parts, $\partial_s\mathscr{P}$ and $\partial_f\mathscr{P}$. Such a subdivision subordinates a partition of the lateral boundary of $\Omega^{(k)}$ into $\partial_s\mathscr{P} \times]-\frac{t}{2}, \frac{t}{2}[= \partial_s\Omega^{(k)}$ and $\partial_f\mathscr{P} \times]-\frac{t}{2}, \frac{t}{2}[= \partial_f\Omega^{(k)}$, where the displacement $\mathbf{s}_0^{(k)}$ and the surface traction $\hat{\mathbf{p}}^{(k)}$ are assigned, respectively. Moreover, the laminated plate is

acted upon by volume forces $\mathbf{b}^{(k)}$, whereas the surface tractions $\mathbf{p}^{\pm}$ are assigned on $\mathscr{P}^{\pm}$.

Each lamina is assumed to be formed by a linearly elastic homogeneous material, having at least a monoclinic symmetry, with symmetry plane parallel to $\mathscr{P}$. In a three-dimensional framework, the constitutive relation for the kth layer can be written as:

$$\boldsymbol{\sigma}^{(k)} = \mathbb{C}^{(k)}\boldsymbol{\varepsilon}^{(k)}, \quad \boldsymbol{\varepsilon}^{(k)} = \mathbb{S}^{(k)}\boldsymbol{\sigma}^{(k)}, \tag{2}$$

where $\boldsymbol{\sigma}^{(k)} = \sigma_{ij}^{(k)}$ and $\boldsymbol{\varepsilon}^{(k)} = \varepsilon_{ij}^{(k)}$ are the second-order stress and strain tensors, respectively; $\mathbb{C}^{(k)} = \mathscr{C}_{ijmh}^{(k)}$ and $\mathbb{S}^{(k)} = (\mathbb{C}^{(k)})^{-1} = \mathscr{S}_{ijmh}^{(k)}$ are the fourth-order elasticity and compliance tensors and they satisfy the major and minor symmetries. Due to the monoclinic assumption $\mathscr{C}_{\alpha\beta\gamma 3}^{(k)} = \mathscr{C}_{33\gamma 3}^{(k)} = \mathscr{S}_{\alpha\beta\gamma 3}^{(k)} = \mathscr{S}_{33\gamma 3}^{(k)} = 0$ and the 13 independent elastic constants of the tensor $\mathbb{C}^{(k)}$ can be tabulated using Voigt's notation as follows:

$$\begin{matrix} \mathscr{C}_{1111}^{(k)} & \mathscr{C}_{1122}^{(k)} & \mathscr{C}_{1133}^{(k)} & 0 & 0 & \mathscr{C}_{1112}^{(k)} \\ & \mathscr{C}_{2222}^{(k)} & \mathscr{C}_{2233}^{(k)} & 0 & 0 & \mathscr{C}_{2212}^{(k)} \\ & & \mathscr{C}_{3333}^{(k)} & 0 & 0 & \mathscr{C}_{3312}^{(k)} \\ & & & \mathscr{C}_{2323}^{(k)} & \mathscr{C}_{2313}^{(k)} & 0 \\ & & & & \mathscr{C}_{1313}^{(k)} & 0 \\ & & & & & \mathscr{C}_{1212}^{(k)}. \end{matrix} \tag{3}$$

Whenever necessary or useful, the standard indicial notation can be used in order to represent vectors or tensors. Moreover, from here onwards, the following notation rules are considered, unless explicitly stated: Greek indices assume values in $\{1,2\}$, whereas Latin indices assume values in $\{1,2,3\}$ with the exception of index n, which assumes values in $\{1,2,3,4\}$. Furthermore, partial derivative of f with respect to the in-plane coordinate x_α is denoted by $f_{,\alpha}$, whereas partial derivative with respect to the thickness coordinate z is indicated with an apex, i.e. f'. Finally, repeated indices are understood to be summed within their ranges, except for the index k, which is used to denote any quantity relative to the kth layer.

The Hu–Washizu functional (cf. [31]), specialized for the case of a laminate, can be written as:

$$\begin{aligned} H(\mathbf{s}^{(k)}, \boldsymbol{\sigma}^{(k)}, \boldsymbol{\varepsilon}^{(k)}) &= \frac{1}{2}\sum_{k=1}^{\ell}\int_{\Omega^{(k)}} \boldsymbol{\varepsilon}^{(k)} : \mathbb{C}^{(k)}\boldsymbol{\varepsilon}^{(k)}\,\mathrm{d}V \\ &+ \sum_{k=1}^{\ell}\int_{\Omega^{(k)}} \boldsymbol{\sigma}^{(k)} : (\nabla^{(\mathrm{s})}\mathbf{s}^{(k)} - \boldsymbol{\varepsilon}^{(k)})\,\mathrm{d}V \\ &- \sum_{k=1}^{\ell}\int_{\Omega^{(k)}} \mathbf{s}^{(k)}\cdot\mathbf{b}^{(k)}\,\mathrm{d}V - \sum_{k=1}^{\ell}\int_{\partial_f\Omega^{(k)}} \mathbf{s}^{(k)}\cdot\hat{\mathbf{p}}^{(k)}\,\mathrm{d}l\,\mathrm{d}z \\ &- \int_{\mathscr{P}} \mathbf{s}^{(1)}\big|_{z_0}\cdot\mathbf{p}^{-}\,\mathrm{d}A - \int_{\mathscr{P}} \mathbf{s}^{(\ell)}\big|_{z_\ell}\cdot\mathbf{p}^{+}\,\mathrm{d}A \\ &- \sum_{k=1}^{\ell}\int_{\partial_s\Omega^{(k)}} (\boldsymbol{\sigma}^{(k)}\mathbf{n})\cdot(\mathbf{s}^{(k)} - \mathbf{s}_0^{(k)})\,\mathrm{d}l\,\mathrm{d}z \\ &+ \sum_{k=1}^{\ell-1}\int_{\mathscr{P}} \left[(\boldsymbol{\sigma}^{(k+1)}\mathbf{e}_3)\cdot(\mathbf{s}^{(k+1)} - \mathbf{s}^{(k)})\right]\big|_{z_k}\mathrm{d}A, \end{aligned} \tag{4}$$

where $\mathbf{s}$ is the displacement vector, $\mathbf{e}_i$ represent the base vectors for the Euclidean space, $\cdot$ and : indicate the scalar vector product and the scalar (second-order) tensor one, respectively; ∇ denotes the gradient operator and superscript (s) denotes the symmetrical part of a tensor. Furthermore, $\cdot|_{z_k}$ is the value of $(\cdot)$ at $z = z_k$, and $\mathrm{d}l$, $\mathrm{d}z$ denote the arc element along $\partial\mathscr{P}$ and the line element along z, respectively.

Stationary conditions of the functional H with respect to $\mathbf{s}^{(k)}$, $\boldsymbol{\sigma}^{(k)}$, $\boldsymbol{\varepsilon}^{(k)}$ yield the equilibrium, compatibility and constitutive equations governing the elastic equilibrium problem for the laminate Ω, regarded as a three-dimensional body.

The mechanical behaviour of moderately thick laminated plates is herein described through a FSDT which takes into account in-plane deformations, bending and first-order shear deformation effects.

The FSDT laminate model is based on the following assumptions on both stress and strain fields: out-of-plane normal stress in the thickness of the plate is null, i.e. $\sigma_{33} = 0$; out-of-plane shear stresses $\sigma_{\alpha 3}$ are continuous piece-wise quadratic functions of the coordinate z; straight lines perpendicular to the mid-plane cannot be stretched and they remain straight, i.e. $\varepsilon_{33} = 0$ and $\varepsilon'_{\alpha 3} = 0$.

It is interesting to recall that, in a general 3D formulation of the elastic problem, the first and the third assumptions are consistent and they can be rationally deduced through the constrained-continua approach (cf. [14]).

In accordance with the assumptions on the strain fields, the displacement field is represented as a linear function of the thickness coordinate z:

$$\mathbf{s}(\mathbf{x}, z) = s_i\mathbf{e}_i = [u_\alpha(\mathbf{x}) + z\varphi_\alpha(\mathbf{x})]\mathbf{e}_\alpha + w(\mathbf{x})\mathbf{e}_3, \tag{5}$$

where $\mathbf{x} = x_\alpha\mathbf{e}_\alpha$ is the in-plane coordinate vector, w is the deflection of the plate mid-plane, $\boldsymbol{\varphi}(\mathbf{x}) = \varphi_\alpha\mathbf{e}_\alpha$ is the rotation vector of fibres parallel to the unit direction $\mathbf{e}_3$ and $\mathbf{u}(\mathbf{x}) = u_\alpha\mathbf{e}_\alpha$ is the in-plane displacement vector (cf. Fig. 1).

Hence, the strain tensor $\boldsymbol{\varepsilon}$ can be decomposed as follows:

$$\boldsymbol{\varepsilon} = \nabla^{(\mathrm{s})}\mathbf{s} = \begin{bmatrix} \overline{\boldsymbol{\varepsilon}} & \frac{1}{2}\boldsymbol{\gamma} \\ \frac{1}{2}\boldsymbol{\gamma}^{\mathrm{T}} & 0 \end{bmatrix}, \tag{6}$$

where the in-plane strain tensor $\overline{\boldsymbol{\varepsilon}} = \varepsilon_{\alpha\beta}\mathbf{e}_\alpha\otimes\mathbf{e}_\beta$ and the shear strain vector $\boldsymbol{\gamma} = 2\varepsilon_{\alpha 3}\mathbf{e}_\alpha$ are defined as:

$$\overline{\boldsymbol{\varepsilon}} = \overline{\nabla}^{(\mathrm{s})}\mathbf{u} + z\overline{\nabla}^{(\mathrm{s})}\boldsymbol{\varphi} = \boldsymbol{\mu} + z\boldsymbol{\omega}, \quad \boldsymbol{\gamma} = \boldsymbol{\varphi} + \overline{\nabla}w \tag{7}$$

with $\overline{\nabla}$ the in-plane gradient operator, i.e. performed with respect to variables x_α, $\boldsymbol{\mu} = \overline{\nabla}^{(\mathrm{s})}\mathbf{u}$ the membranal strain tensor and $\boldsymbol{\omega} = \overline{\nabla}^{(\mathrm{s})}\boldsymbol{\varphi}$ the curvature one.

Introducing the in-plane stress tensor $\overline{\boldsymbol{\sigma}}$, taking into account the stress assumption $\sigma_{33} = 0$ and Eqs. (7), the in-plane stress–strain relation for the kth layer becomes:

$$\overline{\boldsymbol{\sigma}}^{(k)} = \widetilde{\mathbb{C}}^{(k)}\overline{\boldsymbol{\varepsilon}} = \widetilde{\mathbb{C}}^{(k)}(\boldsymbol{\mu} + z\boldsymbol{\omega}), \tag{8}$$

where $\widetilde{\mathbb{C}}^{(k)}$ is the reduced in-plane elasticity tensor, such that $\widetilde{\mathscr{C}}_{\alpha\beta\gamma\delta}^{(k)} = \mathscr{C}_{\alpha\beta\gamma\delta}^{(k)} - \mathscr{C}_{\alpha\beta 33}^{(k)}\mathscr{C}_{\gamma\delta 33}^{(k)}/\mathscr{C}_{3333}^{(k)}$.

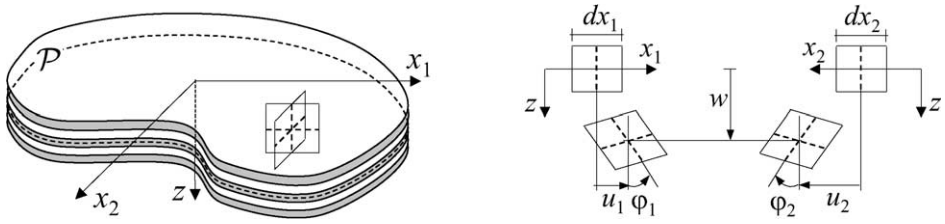


Fig. 1. FSDT laminate model: displacement components.

Furthermore, the transversal shear stress vector $\boldsymbol{\tau} = \sigma_{\alpha 3}\mathbf{e}_\alpha$ can be obtained by the relation:

$$\boldsymbol{\tau}^{(k)} = \widetilde{\mathbf{Q}}^{(k)}\boldsymbol{\gamma}, \tag{9}$$

where $\widetilde{\mathbf{Q}}^{(k)}$ is the second-order shear elastic tensor, defined as (no sum on α and β is performed):

$$\widetilde{\mathscr{Q}}^{(k)}_{\alpha\beta} = \mathscr{C}^{(k)}_{\alpha 3\beta 3}\chi_{\alpha\beta}. \tag{10}$$

The quantities $\chi_{\alpha\beta}$ are the shear correction factors and they are assumed to be constant along the laminate thickness. It can be emphasized that shear factors are not known a priori and values $\chi_{11} = \chi_{22} = 5/6$, $\chi_{12}(=\chi_{21}) = 0$ are strictly correct only for homogeneous plates.

Introducing the resultant stresses as:

$$\mathbf{N} = \sum_{k=1}^{\ell}\int_{z_{k-1}}^{z_k}\overline{\boldsymbol{\sigma}}^{(k)}\,\mathrm{d}z, \quad \mathbf{M} = \sum_{k=1}^{\ell}\int_{z_{k-1}}^{z_k} z\overline{\boldsymbol{\sigma}}^{(k)}\,\mathrm{d}z,$$
$$\mathbf{S} = \sum_{k=1}^{\ell}\int_{z_{k-1}}^{z_k}\boldsymbol{\tau}^{(k)}\,\mathrm{d}z \tag{11}$$

the constitutive equations between $\mathbf{N}$, $\mathbf{M}$, $\mathbf{S}$ and kinematic variables are obtained substituting the local constitutive equations (8) and (9) into (11):

$$\begin{cases}\mathbf{N} = \mathbb{A}\boldsymbol{\mu} + \mathbb{B}\boldsymbol{\omega},\\ \mathbf{M} = \mathbb{B}\boldsymbol{\mu} + \mathbb{D}\boldsymbol{\omega},\\ \mathbf{S} = \mathbf{H}\boldsymbol{\gamma},\end{cases} \tag{12}$$

where the following laminate stiffness tensors are introduced:

$$\mathbb{A} = \sum_{k=1}^{\ell}(z_k - z_{k-1})\widetilde{\mathbb{C}}^{(k)}, \quad \mathbb{B} = \frac{1}{2}\sum_{k=1}^{\ell}(z_k^2 - z_{k-1}^2)\widetilde{\mathbb{C}}^{(k)}, \tag{13}$$

$$\mathbb{D} = \frac{1}{3}\sum_{k=1}^{\ell}(z_k^3 - z_{k-1}^3)\widetilde{\mathbb{C}}^{(k)}, \quad \mathbf{H} = \sum_{k=1}^{\ell}(z_k - z_{k-1})\widetilde{\mathbf{Q}}^{(k)}. \tag{14}$$

Combining Eq. (9) with the third one of (12), the shear stress vector $\boldsymbol{\tau}$ can be expressed as:

$$\boldsymbol{\tau}^{(k)} = \widetilde{\mathbf{Q}}^{(k)}\mathbf{H}^{-1}\mathbf{S}. \tag{15}$$

It is worth observing that $\mathbb{A}, \mathbb{B}$ and $\mathbb{D}$ are respectively the membrane, membrane-bending coupling and bending fourth-order in-plane elasticity tensors, whereas $\mathbf{H}$ represents the resultant elastic shear (second-order) tensor.

Eqs. (12) highlight the great coupling between bending and extension for typical laminated plates. It occurs through the tensor $\mathbb{B}$ and it means that, even though the plate is subjected to a transversal load, in-plane displacements can appear. It is simple to show that if the plate is assumed to be formed by orthotropic layers of equal thickness t/ℓ and considering cross-ply laminates then the coupling tensor $\mathbb{B}$ may be represented as:

$$\begin{cases}\mathscr{B}_{1111} = b = -\mathscr{B}_{2222},\\ \mathscr{B}_{\alpha\alpha\beta\beta} = 0 \quad (\alpha \neq \beta),\\ \mathscr{B}_{\alpha\beta 12} = 0,\end{cases} \tag{16}$$

where b is a material constant which is null for symmetrical lamination sequences. On the other hand, if general laminates are considered and if the layers are assumed with monoclinic constitutive symmetry, the coupling is much more strong. In this cases, the tensor structure of $\mathbb{B}$ is the same of $\widetilde{\mathbb{C}}^{(k)}$.

As the specialistic literature confirms (e.g. [4,20]), a more accurate evaluation of the shear stress vector $\boldsymbol{\tau}$, in comparison with that one derived by the constitutive relation (15), can be obtained through the three-dimensional equilibrium equations.

Accordingly, if no in-plane loads are considered for simplicity (i.e. $b_\alpha = \hat{p}_\alpha = p_\alpha^{\pm} = 0$), the shear stresses in the kth layer are written as:

$$\hat{\boldsymbol{\tau}}^{(k)}(z) = \hat{\boldsymbol{\tau}}_0^{(k)} - \int_{z_{k-1}}^{z}\overline{\nabla}\cdot\overline{\boldsymbol{\sigma}}^{(k)}\,\mathrm{d}\zeta, \tag{17}$$

where $\hat{\boldsymbol{\tau}}_0^{(k)}$ represents the value of the shear stress vector at $z = z_{k-1}$, i.e. $\hat{\boldsymbol{\tau}}_0^{(k)} = \hat{\boldsymbol{\tau}}^{(k)}(z_{k-1})$, with $\hat{\boldsymbol{\tau}}_0^{(1)} = \mathbf{0}$. Now, substituting the in-plane constitutive equation (8) into the expression (17), the function $\hat{\boldsymbol{\tau}}^{(k)}(z)$ for the kth layer can be computed as:

$$\hat{\boldsymbol{\tau}}^{(k)} = \hat{\boldsymbol{\tau}}_0^{(k)} - \int_{z_{k-1}}^{z}\overline{\nabla}\cdot[\widetilde{\mathbb{C}}^{(k)}(\boldsymbol{\mu} + \zeta\boldsymbol{\omega})]\,\mathrm{d}\zeta \tag{18}$$

and in components

$$\hat{\sigma}_{\alpha 3}^{(k)} = \hat{\sigma}_{(0)\alpha 3}^{(k)} - \int_{z_{k-1}}^{z}\frac{\widetilde{\mathscr{C}}^{(k)}_{\alpha\beta\gamma\delta}}{2}[u_{\gamma,\delta\beta} + u_{\delta,\gamma\beta} + \zeta(\varphi_{\gamma,\delta\beta} + \varphi_{\delta,\gamma\beta})]\,\mathrm{d}\zeta. \tag{19}$$

It is worth observing that, in accordance with the kinematical assumptions, in-plain strains are linear functions of the thickness coordinate z and their integrals are quadratic functions layer per layer.

3. A mixed-enhanced finite-element formulation

In this section a mixed-enhanced finite-element formulation for moderately thick laminated plates formed by layers with constitutive monoclinic behaviour is presented.

It is well-known that standard low-order finite elements, i.e. bi-linear displacement-based ones, usually fail the approximations when the plate thickness is numerically small. Nowadays, the reason this lack of convergence (called the shear locking phenomenon) occurs is well-understood (e.g. [23]). As the thickness becomes smaller, the shear energy term degenerates to impose, in the limit $t = 0$, the Kirchhoff constraint (i.e. $\overline{\nabla} w = -\boldsymbol{\varphi}$, e.g. [34]), which is too severe for low-order elements. In order to overcome this drawback several methods have been proposed. Most of them are based on a suitable mixed formulation of the problem, which is able to reduce the influence of the shear energy at the discrete level (e.g. [17]). A different approach consists of improving the approximated deflection space by means of the rotation degrees of freedom. Accordingly, the discrete solution for the transversal displacement is appropriately linked to the rotation one (e.g. [3,37,42]).

In virtue of these considerations and in order to build up a suitable laminate finite element, a partial-mixed formulation is considered. The Kirchhoff condition is accomplished by linking the transversal displacement to the nodal rotations and, in order to avoid locking phenomena, the rotation field is enriched with other modes associated with internal bubble functions. This approach has been proposed for the homogeneous plate by Auricchio and Taylor in [3] and a corresponding error analysis has been presented by Lovadina in [27].

Considering the basic stress and strain FSDT's assumptions and the condition (6), the 3D Hu–Washizu laminate functional (4) can be written in the following form:

$$\begin{aligned} &H(\mathbf{s}, \overline{\boldsymbol{\sigma}}^{(k)}, \boldsymbol{\tau}^{(k)}, \overline{\boldsymbol{\varepsilon}}, \boldsymbol{\gamma}) \\ &\quad = \frac{1}{2}\sum_{k=1}^{\ell}\int_{\Omega^{(k)}} \overline{\boldsymbol{\varepsilon}} : \widetilde{\mathbb{C}}^{(k)}\overline{\boldsymbol{\varepsilon}}\,\mathrm{d}V + \frac{1}{2}\sum_{k=1}^{\ell}\int_{\Omega^{(k)}} \boldsymbol{\tau}^{(k)}\cdot\boldsymbol{\gamma}\,\mathrm{d}V \\ &\qquad + \sum_{k=1}^{\ell}\int_{\Omega^{(k)}} \overline{\boldsymbol{\sigma}}^{(k)} : \left[\overline{\nabla}^{(\mathrm{s})}(\mathbf{P}\mathbf{s}) - \overline{\boldsymbol{\varepsilon}}\right]\mathrm{d}V \\ &\qquad + \sum_{k=1}^{\ell}\int_{\Omega^{(k)}} \overline{\boldsymbol{\tau}}^{(k)}\cdot\left[\mathbf{P}\mathbf{s}' + \overline{\nabla}(\mathbf{s}\cdot\mathbf{e}_3) - \boldsymbol{\gamma}\right]\mathrm{d}V - \Pi_{\mathrm{ext}}, \end{aligned} \tag{20}$$

where Π_{ext} accounts for boundary and loading conditions and $\mathbf{P}$ is an in-plane projector defined as:

$$\mathbf{P} = \begin{bmatrix} 1 & 0 & 0 \\ 0 & 1 & 0 \end{bmatrix}. \tag{21}$$

Substituting the conditions (5) and (7) in (20), performing integration along the thickness coordinate z and taking into account the positions (11)–(14), the functional H can be finally reduced to the following in-plane one:

$$\begin{aligned} &\overline{H}(\mathbf{u}, \boldsymbol{\varphi}, w, \mathbf{N}, \mathbf{M}, \mathbf{S}, \boldsymbol{\mu}, \boldsymbol{\omega}) \\ &\quad = \frac{1}{2}\int_{\mathscr{P}} [\boldsymbol{\mu} : (\mathbb{A}\boldsymbol{\mu} + \mathbb{B}\boldsymbol{\omega}) + \boldsymbol{\omega} : (\mathbb{B}\boldsymbol{\mu} + \mathbb{D}\boldsymbol{\omega})]\,\mathrm{d}A \\ &\qquad + \int_{\mathscr{P}} \left[\mathbf{N} : \left(\overline{\nabla}^{(\mathrm{s})}\mathbf{u} - \boldsymbol{\mu}\right) \mathrm{d}A + \mathbf{M} : \left(\overline{\nabla}^{(\mathrm{s})}\boldsymbol{\varphi} - \boldsymbol{\omega}\right)\right]\mathrm{d}A \\ &\qquad + \int_{\mathscr{P}} \mathbf{S}\cdot\left[\boldsymbol{\varphi} + \overline{\nabla} w - \frac{1}{2}\mathbf{H}^{-1}\mathbf{S}\right]\mathrm{d}A - \Pi_{\mathrm{ext}}. \end{aligned} \tag{22}$$

In the framework of an enhanced-strain formulation (cf. [15,28,36]) the in-plane strain field $\overline{\boldsymbol{\varepsilon}}$ is described as the sum of a compatible contribution $\overline{\nabla}^{(\mathrm{s})}\mathbf{u}$ and of an incompatible one $\overline{\boldsymbol{\varepsilon}}^{\mathrm{en}}(\mathbf{x})$, such that:

$$\boldsymbol{\mu} = \overline{\nabla}^{(\mathrm{s})}\mathbf{u} + \overline{\boldsymbol{\varepsilon}}^{\mathrm{en}}, \quad \boldsymbol{\omega} = \overline{\nabla}^{(\mathrm{s})}\boldsymbol{\varphi}. \tag{23}$$

In other words, in-plain strains arising from the displacement field are "enriched" by means of some additional modes. The most widely adopted enhanced-strain formulations also require the space of the incompatible part of the strain to be orthogonal to the stress one (cf. [15,28]), that is

$$\int_{\Omega} \boldsymbol{\sigma} : \boldsymbol{\varepsilon}^{\mathrm{en}}\,\mathrm{d}V = \sum_{k=1}^{\ell}\int_{\Omega^{(k)}} \overline{\boldsymbol{\sigma}}^{(k)} : \overline{\boldsymbol{\varepsilon}}^{\mathrm{en}}\,\mathrm{d}V = \int_{\mathscr{P}} \mathbf{N} : \overline{\boldsymbol{\varepsilon}}^{\mathrm{en}}\,\mathrm{d}A = 0, \tag{24}$$

where $\varepsilon^{\mathrm{en}}_{\alpha\beta} = \overline{\varepsilon}^{\mathrm{en}}_{\alpha\beta}$ and $\varepsilon^{\mathrm{en}}_{\alpha 3} = 0$.

Using the positions (23) with the in-plane Hu–Washizu functional (22) and enforcing the condition (24), the following partial-mixed enhanced functional is obtained:

$$\begin{aligned} &\overline{H}^{\mathrm{en}}(\mathbf{u}, \boldsymbol{\varphi}, w, \mathbf{S}, \overline{\boldsymbol{\varepsilon}}^{\mathrm{en}}) \\ &\quad = \frac{1}{2}\int_{\mathscr{P}} \left(\overline{\nabla}^{(\mathrm{s})}\mathbf{u} + \overline{\boldsymbol{\varepsilon}}^{\mathrm{en}}\right) : \mathbb{A}\left(\overline{\nabla}^{(\mathrm{s})}\mathbf{u} + \overline{\boldsymbol{\varepsilon}}^{\mathrm{en}}\right)\mathrm{d}A \\ &\qquad + \int_{\mathscr{P}} \left(\overline{\nabla}^{(\mathrm{s})}\mathbf{u} + \overline{\boldsymbol{\varepsilon}}^{\mathrm{en}}\right) : \mathbb{B}\overline{\nabla}^{(\mathrm{s})}\boldsymbol{\varphi}\,\mathrm{d}A \\ &\qquad + \frac{1}{2}\int_{\mathscr{P}} \overline{\nabla}^{(\mathrm{s})}\boldsymbol{\varphi} : \mathbb{D}\overline{\nabla}^{(\mathrm{s})}\boldsymbol{\varphi}\,\mathrm{d}A - \frac{1}{2}\int_{\mathscr{P}} \mathbf{S}\cdot\mathbf{H}^{-1}\mathbf{S}\,\mathrm{d}A \\ &\qquad + \int_{\mathscr{P}} \mathbf{S}\cdot\left(\boldsymbol{\varphi} + \overline{\nabla} w\right)\mathrm{d}A - \Pi_{\mathrm{ext}}. \end{aligned} \tag{25}$$

It is worth observing that imposing the condition $\overline{\boldsymbol{\varepsilon}}^{\mathrm{en}} = \mathbf{0}$ in (25) results in:

$$\begin{aligned} \overline{H}^{\mathrm{en}}|_{\overline{\boldsymbol{\varepsilon}}^{\mathrm{en}}=0} &= \Pi(\mathbf{u}, \boldsymbol{\varphi}, w, \mathbf{S}) \\ &= \Pi^{(\mathrm{mb})}(\mathbf{u}, \boldsymbol{\varphi}) + \Pi^{(\mathrm{s})}(\boldsymbol{\varphi}, w, \mathbf{S}) - \Pi_{\mathrm{ext}}, \end{aligned} \tag{26}$$

where $\Pi^{(\mathrm{mb})}$ contains the bending and extensional terms:

$$\begin{aligned} \Pi^{(\mathrm{mb})}(\mathbf{u}, \boldsymbol{\varphi}) = \frac{1}{2}\int_{\mathscr{P}} \overline{\nabla}^{(\mathrm{s})}\mathbf{u} : \mathbb{A}\overline{\nabla}^{(\mathrm{s})}\mathbf{u}\,\mathrm{d}A + \int_{\mathscr{P}} \overline{\nabla}^{(\mathrm{s})}\mathbf{u} : \mathbb{B}\overline{\nabla}^{(\mathrm{s})}\boldsymbol{\varphi}\,\mathrm{d}A \\ + \frac{1}{2}\int_{\mathscr{P}} \overline{\nabla}^{(\mathrm{s})}\boldsymbol{\varphi} : \mathbb{D}\overline{\nabla}^{(\mathrm{s})}\boldsymbol{\varphi}\,\mathrm{d}A \end{aligned} \tag{27}$$

and $\Pi^{(\mathrm{s})}$ contains the transversal shear terms:

$$\Pi^{(\mathrm{s})}(\boldsymbol{\varphi}, w, \mathbf{S}) = -\frac{1}{2}\int_{\mathscr{P}} \mathbf{S}\cdot\mathbf{H}^{-1}\mathbf{S}\,\mathrm{d}A + \int_{\mathscr{P}} \mathbf{S}\cdot\left(\boldsymbol{\varphi} + \overline{\nabla} w\right)\mathrm{d}A. \tag{28}$$

It is simple to prove (cf. [4]) that functional (26) can be obtained for the above-discussed FSDT laminate model starting from the Hellinger–Reissner mixed functional (e.g. [31]), specialized to the laminate Ω, regarded as a three-dimensional body.

Now, imposing the stationary conditions for the functionals (26) and (25), the following variational problems arise, respectively.

Problem 1. Find $(\mathbf{u},\boldsymbol{\varphi},w,\mathbf{S})\in\mathscr{U}\times\Theta\times\mathscr{W}\times\mathscr{S}$ solution of the following system:

$$\begin{aligned}0&=\mathrm{d}\Pi(\mathbf{u},\boldsymbol{\varphi},w,\mathbf{S})[\delta\mathbf{u}]\\&=\int_{\mathscr{P}}\left(\overline{\nabla}^{(\mathrm{s})}\delta\mathbf{u}\right):\mathbb{A}\overline{\nabla}^{(\mathrm{s})}\mathbf{u}\,\mathrm{d}A+\int_{\mathscr{P}}\left(\overline{\nabla}^{(\mathrm{s})}\delta\mathbf{u}\right):\mathbb{B}\overline{\nabla}^{(\mathrm{s})}\boldsymbol{\varphi}\,\mathrm{d}A\\&\quad\forall\delta\mathbf{u}\in\mathscr{U}\end{aligned}\tag{29}$$

$$\begin{aligned}0&=\mathrm{d}\Pi(\mathbf{u},\boldsymbol{\varphi},w,\mathbf{S})[(\delta\boldsymbol{\varphi},\delta w)]\\&=\int_{\mathscr{P}}\left(\overline{\nabla}^{(\mathrm{s})}\delta\boldsymbol{\varphi}\right):\mathbb{B}\overline{\nabla}^{(\mathrm{s})}\mathbf{u}\,\mathrm{d}A+\int_{\mathscr{P}}\left(\overline{\nabla}^{(\mathrm{s})}\delta\boldsymbol{\varphi}\right):\mathbb{D}\overline{\nabla}^{(\mathrm{s})}\boldsymbol{\varphi}\,\mathrm{d}A\\&\quad+\int_{\mathscr{P}}\mathbf{S}\cdot\left(\delta\boldsymbol{\varphi}+\overline{\nabla}\delta w\right)\mathrm{d}A-\int_{\mathscr{P}}q\,\delta w\,\mathrm{d}A\\&\quad\forall(\delta\boldsymbol{\varphi},\delta w)\in\Theta\times\mathscr{W}\end{aligned}\tag{30}$$

$$\begin{aligned}0&=\mathrm{d}\Pi(\mathbf{u},\boldsymbol{\varphi},w,\mathbf{S})[\delta\mathbf{S}]\\&=\int_{\mathscr{P}}\delta\mathbf{S}\cdot(\boldsymbol{\varphi}+\overline{\nabla}w)\,\mathrm{d}A-\int_{\mathscr{P}}\delta\mathbf{S}\cdot\mathbf{H}^{-1}\mathbf{S}\,\mathrm{d}A\\&\quad\forall\delta\mathbf{S}\in\mathscr{S}.\end{aligned}\tag{31}$$

Problem 2. Find $(\mathbf{u},\boldsymbol{\varphi},w,\mathbf{S},\overline{\boldsymbol{\varepsilon}}^{\mathrm{en}})\in\mathscr{U}\times\Theta\times\mathscr{W}\times\mathscr{S}\times\mathscr{E}$ solution of the following system:

$$\begin{aligned}0&=\mathrm{d}\overline{H}^{\mathrm{en}}(\mathbf{u},\boldsymbol{\varphi},w,\mathbf{S},\overline{\boldsymbol{\varepsilon}}^{\mathrm{en}})[\delta\mathbf{u}]\\&=\mathrm{d}\Pi(\mathbf{u},\boldsymbol{\varphi},w,\mathbf{S})[\delta\mathbf{u}]+\int_{\mathscr{P}}\left(\overline{\nabla}^{(\mathrm{s})}\delta\mathbf{u}\right):\mathbb{A}\overline{\boldsymbol{\varepsilon}}^{\mathrm{en}}\,\mathrm{d}A\\&\quad\forall\delta\mathbf{u}\in\mathscr{U}\end{aligned}\tag{32}$$

$$\begin{aligned}0&=\mathrm{d}\overline{H}^{\mathrm{en}}(\mathbf{u},\boldsymbol{\varphi},w,\mathbf{S},\overline{\boldsymbol{\varepsilon}}^{\mathrm{en}})[(\delta\boldsymbol{\varphi},\delta w)]\\&=\mathrm{d}\Pi(\mathbf{u},\boldsymbol{\varphi},w,\mathbf{S})[(\delta\boldsymbol{\varphi},\delta w)]+\int_{\mathscr{P}}\left(\overline{\nabla}^{(\mathrm{s})}\delta\boldsymbol{\varphi}\right):\mathbb{B}\overline{\boldsymbol{\varepsilon}}^{\mathrm{en}}\,\mathrm{d}A\\&\quad\forall(\delta\boldsymbol{\varphi},\delta w)\in\Theta\times\mathscr{W}\end{aligned}\tag{33}$$

$$\begin{aligned}0&=\mathrm{d}\overline{H}^{\mathrm{en}}(\mathbf{u},\boldsymbol{\varphi},w,\mathbf{S},\overline{\boldsymbol{\varepsilon}}^{\mathrm{en}})[\delta\mathbf{S}]=\mathrm{d}\Pi(\mathbf{u},\boldsymbol{\varphi},w,\mathbf{S})[\delta\mathbf{S}]\\&\quad\forall\delta\mathbf{S}\in\mathscr{S}\end{aligned}\tag{34}$$

$$\begin{aligned}0&=\mathrm{d}\overline{H}^{\mathrm{en}}(\mathbf{u},\boldsymbol{\varphi},w,\mathbf{S},\overline{\boldsymbol{\varepsilon}}^{\mathrm{en}})[\delta\overline{\boldsymbol{\varepsilon}}^{\mathrm{en}}]\\&=\int_{\mathscr{P}}\delta\overline{\boldsymbol{\varepsilon}}^{\mathrm{en}}:\mathbb{A}\left(\overline{\nabla}^{(\mathrm{s})}\mathbf{u}+\overline{\boldsymbol{\varepsilon}}^{\mathrm{en}}\right)\mathrm{d}A+\int_{\mathscr{P}}\delta\overline{\boldsymbol{\varepsilon}}^{\mathrm{en}}:\mathbb{B}\overline{\nabla}^{(\mathrm{s})}\boldsymbol{\varphi}\,\mathrm{d}A\\&\quad\forall\delta\overline{\boldsymbol{\varepsilon}}^{\mathrm{en}}\in\mathscr{E}.\end{aligned}\tag{35}$$

As notation rules, $\delta\mathbf{u}$, for example, indicates a possible variation of the field $\mathbf{u}$ and $\mathrm{d}\Pi(\mathbf{u},\boldsymbol{\varphi},w,\mathbf{S})[\delta\mathbf{u}]$ indicates the variation of Π evaluated at $(\mathbf{u},\boldsymbol{\varphi},w,\mathbf{S})$ in the direction $\delta\mathbf{u}$. The previous problems have been formalized considering, for simplicity, the case of a clamped laminated plate, subjected to a transversal load $q(\mathbf{x})$. Moreover, with reference to a standard notation (cf. [16]), the following spaces have been introduced: $\mathscr{U}=H_0^1(\mathscr{P})^2$, $\Theta=H_0^1(\mathscr{P})^2$, $\mathscr{W}=H_0^1(\mathscr{P})$, $\mathscr{S}=L^2(\mathscr{P})$, whereas $\mathscr{E}$ is the space of symmetric tensors $\varepsilon_{\alpha\beta}$ with components in $L^2(\mathscr{P})$ (i.e. $L^2(\mathscr{P})_s^4$) and which respects the condition (24).

Auricchio et al. in [6] show that the Problem 1 admits a unique solution $(\tilde{\mathbf{u}},\tilde{\boldsymbol{\varphi}},\tilde{w},\widetilde{\mathbf{S}})\in\mathscr{U}\times\Theta\times\mathscr{W}\times\mathscr{S}$. Moreover, they show that as t tends to zero $(\tilde{\mathbf{u}},\tilde{w})$ converges to $(\mathbf{u}_o,w_o)\in H_0^1(\mathscr{P})^2\times H_0^2(\mathscr{P})$, the solution of the Kirchhoff-type laminated plate problem.

Now, considering the solution of the Problem 1 and combining the conditions (29)–(31) with (32)–(35), Problem 2 reduces to:

$$\begin{aligned}&\int_{\mathscr{P}}(\overline{\nabla}^{(\mathrm{s})}\delta\mathbf{u}):\mathbb{A}\overline{\boldsymbol{\varepsilon}}^{\mathrm{en}}\,\mathrm{d}A=0\quad\forall\delta\mathbf{u}\in\mathscr{U},\\&\int_{\mathscr{P}}(\overline{\nabla}^{(\mathrm{s})}\delta\boldsymbol{\varphi}):\mathbb{B}\overline{\boldsymbol{\varepsilon}}^{\mathrm{en}}\,\mathrm{d}A=0\quad\forall(\delta\boldsymbol{\varphi},w)\in\Theta\times\mathscr{W},\\&\int_{\mathscr{P}}\delta\overline{\boldsymbol{\varepsilon}}^{\mathrm{en}}:\mathscr{A}\overline{\boldsymbol{\varepsilon}}^{\mathrm{en}}\,\mathrm{d}A=0\quad\forall\delta\overline{\boldsymbol{\varepsilon}}^{\mathrm{en}}\in\mathscr{E}.\end{aligned}\tag{36}$$

Accordingly, $(\tilde{\mathbf{u}},\tilde{\boldsymbol{\varphi}},\tilde{w},\widetilde{\mathbf{S}},\mathbf{0})$ represents the unique solution for the enhanced variational Problem 2, i.e. in solution $\boldsymbol{\mu}=\overline{\nabla}^{(\mathrm{s})}\mathbf{u}$ (cf. Eq. (23)).

The functional (25) is considered as a starting point for the development of the finite-element scheme and a partial-mixed approach is adopted. The bi-linear shape functions (cf. [43]) are used to map the parent domain with natural coordinates (ξ,η) to the real domain with coordinates (x_1,x_2). As a consequence, the quadrilateral region occupied by each element may be expressed by:

$$\mathbf{x}=\Psi_n\hat{\mathbf{x}}_n=\frac{1}{4}(1+\xi\xi_n)(1+\eta\eta_n)\hat{\mathbf{x}}_n=\boldsymbol{\Psi}\hat{\mathbf{x}},\tag{37}$$

where $\mathbf{x}=\{x_1,x_2\}^{\mathrm{T}}$ denotes any point in the element, $\hat{\mathbf{x}}_n=\{\hat{x}_{n1},\hat{x}_{n2}\}^{\mathrm{T}}$ are the coordinates at node n, $\hat{\mathbf{x}}$ is the nodal coordinates vector, Ψ_n are the bi-linear shape functions, with (ξ_n,η_n) being the values of the natural coordinates at node n.

The in-plane displacements are taken bi-linear in the nodal parameters $\hat{\mathbf{u}}$:

$$\mathbf{u}=\boldsymbol{\Psi}\hat{\mathbf{u}}.\tag{38}$$

The interpolation for the rotation field is bi-linear in the nodal parameters $\hat{\boldsymbol{\varphi}}$, with added internal degrees of freedom $\hat{\boldsymbol{\varphi}}^{(\mathrm{b})}$:

$$\boldsymbol{\varphi}=\boldsymbol{\Psi}\hat{\boldsymbol{\varphi}}+\boldsymbol{\Psi}^{(\mathrm{b})}\hat{\boldsymbol{\varphi}}^{(\mathrm{b})},\tag{39}$$

where $\boldsymbol{\Psi}^{(b)}$ are bubble functions defined as (cf. [3]):

$$\boldsymbol{\Psi}^{(\mathrm{b})}=\frac{(1-\xi^2)(1-\eta^2)}{j}\begin{bmatrix}J_{22}^0 & -J_{12}^0 & J_{22}^0\eta & -J_{12}^0\xi\\ -J_{21}^0 & J_{11}^0 & -J_{21}^0\eta & J_{11}^0\xi\end{bmatrix}\tag{40}$$

being $\mathbf{J}_0$ the Jacobian of the isoparametric mapping evaluated at $\xi=\eta=0$:

$$J_{i1}^0=\left.\frac{\partial x_i}{\partial\xi}\right|_{\xi=\eta=0},\quad J_{i2}^0=\left.\frac{\partial x_i}{\partial\eta}\right|_{\xi=\eta=0}\tag{41}$$

and $j=\det[\mathbf{J}]$ the Jacobian determinant.

The transversal displacement interpolation is bi-linear in the nodal parameters $\hat{\mathbf{w}}$, enriched with linked quadratic functions expressed in terms of nodal rotations $\hat{\boldsymbol{\varphi}}$:

$$w = \Psi_n \hat{w}_n + \Psi_n^{(w\varphi)} L_n (\hat{\varphi}_n^o - \hat{\varphi}_s^o), \tag{42}$$

where $\hat{\varphi}_n^o$ and $\hat{\varphi}_s^o$ represents the rotations of the nodes n and s in the directions normal to the $n-s$ side, whose length is L_n. Moreover, in order to have constant transversal shear along each side of the element the shape functions $\Psi_n^{(w\varphi)}$ are defined as (cf. [3]):

$$\boldsymbol{\Psi}^{(w\varphi)} = \begin{Bmatrix} \Psi_1^{(w\varphi)} \\ \Psi_2^{(w\varphi)} \\ \Psi_3^{(w\varphi)} \\ \Psi_4^{(w\varphi)} \end{Bmatrix} = \frac{1}{16} \begin{Bmatrix} (1-\xi^2)(1-\eta) \\ (1+\xi)(1-\eta^2) \\ (1-\xi^2)(1+\eta) \\ (1-\xi)(1-\eta^2) \end{Bmatrix}. \tag{43}$$

The shear interpolation is also bi-linear and defined locally to each element as:

$$\mathbf{S} = \boldsymbol{\Psi}^{(S)} \widehat{\mathbf{S}} = \begin{bmatrix} J_{11}^0 & J_{21}^0 & J_{11}^0 \eta & J_{21}^0 \xi \\ J_{12}^0 & J_{22}^0 & J_{12}^0 \eta & J_{22}^0 \xi \end{bmatrix} \begin{Bmatrix} S_1 \\ S_2 \\ S_3 \\ S_4 \end{Bmatrix} \tag{44}$$

with $\widehat{\mathbf{S}}$ parameters local to each element.

Finally, the symmetrical enhanced strain field $\overline{\boldsymbol{\varepsilon}}^{\mathrm{en}}$, using its equivalent vectorial field $\overline{\mathbf{e}}^{\mathrm{en}}$, is expressed as:

$$\overline{\mathbf{e}}^{\mathrm{en}} = \boldsymbol{\Gamma} \hat{\boldsymbol{\varepsilon}}^{\mathrm{en}}, \tag{45}$$

where $\hat{\boldsymbol{\varepsilon}}^{\mathrm{en}}$ is a set of internal degrees of freedom local to each element and $\boldsymbol{\Gamma}$ is an interpolation matrix.

Following Ref. [36], $\boldsymbol{\Gamma}$ is constructed mapping an interpolation matrix $\boldsymbol{\Gamma}^p$, defined on the parent element, into the physical one using the formula:

$$\boldsymbol{\Gamma} = \frac{j_0}{j} \mathbf{F}_0^{-\mathrm{T}} \boldsymbol{\Gamma}^p, \tag{46}$$

where $j_0 = j|_{\xi=\eta=0}$ and

$$\mathbf{F}_0 = \begin{bmatrix} J_{11}^2 & J_{12}^2 & 2J_{11}J_{12} \\ J_{21}^2 & J_{22}^2 & 2J_{21}J_{22} \\ J_{11}J_{21} & J_{12}J_{22} & J_{11}J_{22} + J_{12}J_{21} \end{bmatrix}_{\xi=\eta=0}. \tag{47}$$

With regards the choice of the matrix $\boldsymbol{\Gamma}$, it can be observed that the enhanced strain $\overline{\boldsymbol{\varepsilon}}^{\mathrm{en}}$ should improve the in-plane compatible interpolation. This is usually done guaranteeing that the polynomials in $\boldsymbol{\Gamma}$ are not already contained in the compatible strains. Moreover, due to the presence of the non-zero constitutive tensor $\mathbb{B}$, the total in-plane deformation $\boldsymbol{\mu} = \overline{\nabla}^{(\mathrm{s})}\mathbf{u} + \overline{\boldsymbol{\varepsilon}}^{\mathrm{en}}$ is coupled with the curvature field $\boldsymbol{\omega} = \overline{\nabla}^{(\mathrm{s})}\boldsymbol{\varphi}$. As a consequence, the in-plane and the rotation interpolations cannot be independent. In detail, as suggested in [5], the interpolation matrix $\boldsymbol{\Gamma}$ should be able to satisfy the discretized form of Eq. $(12)_1$ for $\mathbf{N} = \mathbf{0}$:

$$\mathbf{A}(\mathbf{e} + \boldsymbol{\Gamma}\hat{\boldsymbol{\varepsilon}}^{\mathrm{en}}) + \mathbf{B}\boldsymbol{\vartheta} = \mathbf{0}, \tag{48}$$

where $\mathbf{A}$ and $\mathbf{B}$ are the matrices associated with the tensors $\mathbb{A}$ and $\mathbb{B}$, whereas $\mathbf{e}$ and $\boldsymbol{\vartheta}$ are the vectors associated with the discretized form of tensors $\overline{\nabla}^{(\mathrm{s})}\mathbf{u}$ and $\overline{\nabla}^{(\mathrm{s})}\boldsymbol{\varphi}$, respectively.

It can be useful to recall that a symmetrical fourth-order in-plane tensor $\mathbb{F}$ may be represented as the 3×3 matrix $\mathbf{F}$, whereas a symmetrical second-order in-plane tensor $\boldsymbol{\theta}$ may be represented as the vector $\mathbf{q}$, being $\mathbb{F}$ and $\mathbf{q}$ defined as:

$$\begin{cases} F_{\alpha\beta} = \mathscr{F}_{\alpha\alpha\beta\beta}, \\ F_{\alpha 3} = \mathscr{F}_{\alpha\alpha 12}, \\ F_{33} = \mathscr{F}_{1212}, \end{cases} \quad \begin{cases} q_\alpha = \theta_{\alpha\alpha}, \\ q_3 = 2\theta_{12}. \end{cases} \tag{49}$$

Taking into account the above-introduced interpolation schemes, results in:

$$2(\overline{\nabla}^{(\mathrm{s})}\mathbf{u})_{\alpha\beta} = \Psi_{n,\alpha}\hat{u}_{n\beta} + \Psi_{n,\beta}\hat{u}_{n\alpha}, \tag{50}$$

$$2(\overline{\nabla}^{(\mathrm{s})}\boldsymbol{\varphi})_{\alpha\beta} = \Psi_{n,\alpha}\hat{\varphi}_{n\beta} + \Psi_{n,\beta}\hat{\varphi}_{n\alpha} + (\Psi^{(\mathrm{b})}_{\alpha n,\beta} + \Psi^{(\mathrm{b})}_{\beta n,\alpha})\hat{\varphi}_n^{(\mathrm{b})}. \tag{51}$$

Hence, introducing the operator

$$\mathbf{L} = \begin{bmatrix} \frac{\partial\cdot}{\partial x_1} & 0 \\ 0 & \frac{\partial\cdot}{\partial x_2} \\ \frac{\partial\cdot}{\partial x_1} & \frac{\partial\cdot}{\partial x_2} \end{bmatrix} \tag{52}$$

results in:

$$\mathbf{e} = \mathbf{L}\mathbf{u} = \mathbf{L}\boldsymbol{\Psi}\hat{\mathbf{u}}, \quad \boldsymbol{\vartheta} = \mathbf{L}\boldsymbol{\varphi} = \mathbf{L}\boldsymbol{\Psi}\hat{\boldsymbol{\varphi}} + \mathbf{L}\boldsymbol{\Psi}^{(\mathrm{b})}\hat{\boldsymbol{\varphi}}^{(\mathrm{b})}. \tag{53}$$

After some calculation, the consistency condition (48) leads to the following choice for $\boldsymbol{\Gamma}_p$:

$$\boldsymbol{\Gamma}_p = \begin{bmatrix} \xi & 0 & 0 & 0 & \xi\eta & \mathbf{g} & \mathbf{0} & \mathbf{0} \\ 0 & \eta & 0 & 0 & -\xi\eta & \mathbf{0} & \mathbf{g} & \mathbf{0} \\ 0 & 0 & \xi & \eta & \xi^2-\eta^2 & \mathbf{0} & \mathbf{0} & \mathbf{g} \end{bmatrix}, \tag{54}$$

where $\mathbf{g} = \{\xi\eta_2, \eta\xi_2, \xi\eta\eta_2, \xi\eta\xi_2, \xi^2, \eta^2, \eta^2\xi_2, \xi^2\eta_2\}$, with $\xi_2 = (1-\xi^2)$ and $\eta_2 = (1-\eta^2)$.

The interpolation matrix proposed in (54) refers to the case of laminates formed by monoclinic layers and it generalizes that one discussed in [5], which is strictly valid only in the case of orthotropic cross-ply laminates.

Introducing the above interpolation schemes and performing the stationary conditions of the functional (25) for a single element of area A_{e}, the following algebraic system is obtained:

$$\begin{bmatrix} \mathbf{K}_{uu} & \mathbf{0} & \mathbf{K}_{u\varphi} & \mathbf{K}_{ub} & \mathbf{0} & \mathbf{K}_{\varepsilon u}^{\mathrm{T}} \\ \mathbf{0} & \mathbf{0} & \mathbf{0} & \mathbf{0} & \mathbf{K}_{Sw}^{\mathrm{T}} & \mathbf{0} \\ \mathbf{K}_{u\varphi}^{\mathrm{T}} & \mathbf{0} & \mathbf{K}_{\varphi\varphi} & \mathbf{K}_{b\varphi}^{\mathrm{T}} & \mathbf{K}_{S\varphi}^{\mathrm{T}} & \mathbf{K}_{\varepsilon\varphi}^{\mathrm{T}} \\ \mathbf{K}_{ub}^{\mathrm{T}} & \mathbf{0} & \mathbf{K}_{b\varphi} & \mathbf{K}_{bb} & \mathbf{K}_{bS} & \mathbf{K}_{\varepsilon b}^{\mathrm{T}} \\ \mathbf{0} & \mathbf{K}_{Sw} & \mathbf{K}_{S\varphi} & \mathbf{K}_{bS}^{\mathrm{T}} & \mathbf{K}_{SS} & \mathbf{0} \\ \mathbf{K}_{\varepsilon u} & \mathbf{0} & \mathbf{K}_{\varepsilon\varphi} & \mathbf{K}_{\varepsilon b} & \mathbf{0} & \mathbf{K}_{\varepsilon\varepsilon}^{\mathrm{T}} \end{bmatrix} \begin{Bmatrix} \hat{\mathbf{u}} \\ \hat{w} \\ \hat{\boldsymbol{\varphi}} \\ \hat{\boldsymbol{\varphi}}^{(\mathrm{b})} \\ \hat{\mathbf{S}} \\ \hat{\boldsymbol{\varepsilon}}^{\mathrm{en}} \end{Bmatrix} = \begin{Bmatrix} \hat{\mathbf{f}}_u \\ \hat{\mathbf{f}}_w \\ \hat{\mathbf{f}}_\varphi \\ \mathbf{0} \\ \mathbf{0} \\ \mathbf{0} \end{Bmatrix}, \tag{55}$$

where the right side contains the terms due to loads and boundary conditions. The submatrices in (55) are given by:

$$\begin{aligned}
&\mathbf{K}_{uu} = \int_{A_e} (\mathbf{L}\boldsymbol{\Psi})^{\mathrm{T}} \mathbf{A} (\mathbf{L}\boldsymbol{\Psi}) \,\mathrm{d}A, && \mathbf{K}_{u\varphi} = \int_{A_e} (\mathbf{L}\boldsymbol{\Psi})^{\mathrm{T}} \mathbf{B} (\mathbf{L}\boldsymbol{\Psi}) \,\mathrm{d}A,\\
&\mathbf{K}_{\varphi\varphi} = \int_{A_e} (\mathbf{L}\boldsymbol{\Psi})^{\mathrm{T}} \mathbf{D} (\mathbf{L}\boldsymbol{\Psi}) \,\mathrm{d}A, && \mathbf{K}_{bu} = \int_{A_e} (\mathbf{L}\boldsymbol{\Psi}^{(\mathrm{b})})^{\mathrm{T}} \mathbf{B} (\mathbf{L}\boldsymbol{\Psi}) \,\mathrm{d}A,\\
&\mathbf{K}_{b\varphi} = \int_{A_e} (\mathbf{L}\boldsymbol{\Psi}_b)^{\mathrm{T}} \mathbf{D} (\mathbf{L}\boldsymbol{\Psi}) \,\mathrm{d}A, && \mathbf{K}_{bb} = \int_{A_e} (\mathbf{L}\boldsymbol{\Psi}_b)^{\mathrm{T}} \mathbf{D} (\mathbf{L}\boldsymbol{\Psi}_b) \,\mathrm{d}A,\\
&\mathbf{K}_{bS} = \int_{A_e} (\boldsymbol{\Psi}_b)^{\mathrm{T}} \boldsymbol{\Psi}_S \,\mathrm{d}A, && \mathbf{K}_{Sw} = \int_{A_e} (\boldsymbol{\Psi}_S)^{\mathrm{T}} (\overline{\nabla} \boldsymbol{\Psi}) \,\mathrm{d}A,\\
&\mathbf{K}_{S\varphi} = \int_{A_e} (\boldsymbol{\Psi}_S)^{\mathrm{T}} (\boldsymbol{\Psi} + \overline{\nabla} \boldsymbol{\Psi}^{(w\varphi)}) \,\mathrm{d}A, && \mathbf{K}_{bb} = \int_{A_e} (\mathbf{L}\boldsymbol{\Psi}^{(\mathrm{b})})^{\mathrm{T}} \mathbf{D} (\mathbf{L}\boldsymbol{\Psi}^{(\mathrm{b})}) \,\mathrm{d}A,
\end{aligned} \tag{56}$$

where $\mathbf{A}$, $\mathbf{B}$ and $\mathbf{D}$ are the matrices associated to the tensors $\mathbb{A}$, $\mathbb{B}$ and $\mathbb{D}$, respectively.

Since the enhanced strain, the bubble rotation and the resultant shear stress are local parameters to each element, they can be eliminated by static condensation. Performing the condensation in order with respect to $\hat{\boldsymbol{\varepsilon}}^{\mathrm{en}}$, $\hat{\boldsymbol{\varphi}}_b$, $\widehat{\boldsymbol{S}}$, the following system is obtained:

$$\begin{bmatrix} \overline{\mathbf{K}}_{uu} & \overline{\mathbf{K}}_{uw} & \overline{\mathbf{K}}_{u\varphi} \\ \overline{\mathbf{K}}_{uw}^{\mathrm{T}} & \overline{\mathbf{K}}_{ww} & \overline{\mathbf{K}}_{w\varphi} \\ \overline{\mathbf{K}}_{u\varphi}^{\mathrm{T}} & \overline{\mathbf{K}}_{w\varphi} & \overline{\mathbf{K}}_{\varphi\varphi} \end{bmatrix} \begin{Bmatrix} \hat{\mathbf{u}} \\ \hat{\mathbf{w}} \\ \hat{\boldsymbol{\varphi}} \end{Bmatrix} = \begin{Bmatrix} \hat{\mathbf{f}}_u \\ \hat{\mathbf{f}}_w \\ \hat{\mathbf{f}}_\varphi \end{Bmatrix}, \tag{57}$$

where the corresponding submatrices are obtained through algebraic manipulations of (56):

$$\begin{aligned}
&\overline{\mathbf{K}}_{uu} = \widetilde{\mathbf{K}}_{uu} - \widetilde{\mathbf{K}}_{Su}^{\mathrm{T}} \widetilde{\mathbf{K}}_{SS}^{-1} \widetilde{\mathbf{K}}_{Su}, && \overline{\mathbf{K}}_{uw} = -\widetilde{\mathbf{K}}_{Su}^{\mathrm{T}} \widetilde{\mathbf{K}}_{SS}^{-1} \widetilde{\mathbf{K}}_{Sw},\\
&\overline{\mathbf{K}}_{u\varphi} = \widetilde{\mathbf{K}}_{u\varphi} - \widetilde{\mathbf{K}}_{Su}^{\mathrm{T}} \widetilde{\mathbf{K}}_{SS}^{-1} \widetilde{\mathbf{K}}_{S\varphi}, && \overline{\mathbf{K}}_{ww} = -\widetilde{\mathbf{K}}_{wS}^{\mathrm{T}} \widetilde{\mathbf{K}}_{SS}^{-1} \widetilde{\mathbf{K}}_{Sw},\\
&\overline{\mathbf{K}}_{w\varphi} = -\widetilde{\mathbf{K}}_{wS}^{\mathrm{T}} \widetilde{\mathbf{K}}_{SS}^{-1} \widetilde{\mathbf{K}}_{S\varphi}, && \overline{\mathbf{K}}_{\varphi\varphi} = \widetilde{\mathbf{K}}_{\varphi\varphi} - \widetilde{\mathbf{K}}_{\varphi S} \widetilde{\mathbf{K}}_{SS}^{-1} \widetilde{\mathbf{K}}_{S\varphi},
\end{aligned} \tag{58}$$

$$\begin{aligned}
&\widetilde{\mathbf{K}}_{uu} = \underline{\mathbf{K}}_{uu} - \underline{\mathbf{K}}_{bu}^{\mathrm{T}} \underline{\mathbf{K}}_{bb}^{-1} \underline{\mathbf{K}}_{bu}, && \widetilde{\mathbf{K}}_{u\varphi} = \underline{\mathbf{K}}_{u\varphi} - \underline{\mathbf{K}}_{bu}^{\mathrm{T}} \underline{\mathbf{K}}_{bb}^{-1} \underline{\mathbf{K}}_{b\varphi},\\
&\widetilde{\mathbf{K}}_{\varphi\varphi} = \underline{\mathbf{K}}_{\varphi\varphi} - \underline{\mathbf{K}}_{b\varphi}^{\mathrm{T}} \underline{\mathbf{K}}_{bb}^{-1} \underline{\mathbf{K}}_{b\varphi}, && \widetilde{\mathbf{K}}_{Su} = -\underline{\mathbf{K}}_{bS}^{\mathrm{T}} \underline{\mathbf{K}}_{bb}^{-1} \underline{\mathbf{K}}_{bu},\\
&\widetilde{\mathbf{K}}_{Sw} = \underline{\mathbf{K}}_{Sw}, && \widetilde{\mathbf{K}}_{S\varphi} = \underline{\mathbf{K}}_{S\varphi} - \underline{\mathbf{K}}_{bS}^{\mathrm{T}} \underline{\mathbf{K}}_{bb}^{-1} \underline{\mathbf{K}}_{b\varphi},\\
&\widetilde{\mathbf{K}}_{SS} = \underline{\mathbf{K}}_{SS} - \underline{\mathbf{K}}_{bS}^{\mathrm{T}} \underline{\mathbf{K}}_{bb}^{-1} \underline{\mathbf{K}}_{bS},
\end{aligned} \tag{59}$$

$$\begin{aligned}
&\underline{\mathbf{K}}_{uu} = \mathbf{K}_{uu} - \mathbf{K}_{\varepsilon u}^{\mathrm{T}} \mathbf{K}_{\varepsilon\varepsilon}^{-1} \mathbf{K}_{\varepsilon u}, && \underline{\mathbf{K}}_{u\varphi} = \mathbf{K}_{u\varphi} - \mathbf{K}_{u\varphi}^{\mathrm{T}} \mathbf{K}_{\varepsilon\varepsilon}^{-1} \mathbf{K}_{\varepsilon\varphi},\\
&\underline{\mathbf{K}}_{\varphi\varphi} = \mathbf{K}_{\varphi\varphi} - \mathbf{K}_{\varepsilon\varphi}^{\mathrm{T}} \mathbf{K}_{\varepsilon\varepsilon}^{-1} \mathbf{K}_{\varepsilon\varphi}, && \underline{\mathbf{K}}_{bu} = \mathbf{K}_{bu} - \mathbf{K}_{\varepsilon b}^{\mathrm{T}} \mathbf{K}_{\varepsilon\varepsilon}^{-1} \mathbf{K}_{\varepsilon u},\\
&\underline{\mathbf{K}}_{b\varphi} = \mathbf{K}_{b\varphi} - \mathbf{K}_{\varepsilon b}^{\mathrm{T}} \mathbf{K}_{\varepsilon\varepsilon}^{-1} \mathbf{K}_{\varepsilon\varphi}, && \underline{\mathbf{K}}_{bb} = \mathbf{K}_{bb} - \mathbf{K}_{\varepsilon b}^{\mathrm{T}} \mathbf{K}_{\varepsilon\varepsilon}^{-1} \mathbf{K}_{\varepsilon b}\\
&\underline{\mathbf{K}}_{bS} = \mathbf{K}_{bS}, && \underline{\mathbf{K}}_{Sw} = \mathbf{K}_{Sw},\\
&\underline{\mathbf{K}}_{S\varphi} = \mathbf{K}_{S\varphi}, && \underline{\mathbf{K}}_{SS} = \mathbf{K}_{SS}.
\end{aligned} \tag{60}$$

Accordingly, an element with five global degrees of freedom per node is obtained. This laminate element is named MEML4 to remind that it is a Monoclinic Enhanced Mixed Linked 4-node finite element.

It is worth observing that the invertibility of $\mathbf{K}_{SS}$ is not required during the algebraic manipulations. On the other hand, it is necessary to compute the inverse of $\widetilde{\mathbf{K}}_{SS}$, which is not singular even for zero shear compliance. This is obtained by proper selection of the shape bubble functions. Any problem converging to the thin plate case can be investigated, without the problem becoming ill-conditioned. Similarly, the shear energy can be included or excluded from the analysis as an optional element feature.

Due to the adopted mixed formulation, an accurate evaluation of the resultant shear stress $\mathbf{S}$ is expected and, as a consequence, this occurrence leads to the possibility of shear stress profiles improving. Since in the finite-element scheme the equilibrium equations are not locally satisfied, the direct use of Eq. (18) does not allow a satisfactory recovery of the shear stress profiles. Therefore, the shear stress profiles can be evaluated solving the following minimization problem:

$$\min \left\{ \left\| \hat{\boldsymbol{\tau}}^{(k)}(x_3) - \hat{\boldsymbol{\tau}}_0^{(k)} + \int_{x_3^{(k-1)}}^{x_3} \overline{\nabla} \cdot [\widetilde{\mathbb{C}}^{(k)} (\mathbf{E} + \zeta \boldsymbol{\Theta})] \,\mathrm{d}\zeta \right\| \right\} \tag{61}$$

subjected to the constraints:

$$\hat{\boldsymbol{\tau}}|_{\pm t/2} = \mathbf{0}, \quad \int_{-t/2}^{t/2} \hat{\boldsymbol{\tau}} \,\mathrm{d}x_3 - \mathbf{S} = \mathbf{0}, \tag{62}$$

where $\|\cdot\|$ represents a given norm.

In detail, the shear stresses are numerically computed through the following formula:

$$\begin{aligned}
\boldsymbol{\tau}^{(k)}(z) = \begin{bmatrix} b_1 & 0 \\ 0 & b_2 \end{bmatrix} \Bigg[& -\frac{1}{2}(z^2 - z_{k-1}^2) \mathbf{L}^{\mathrm{T}} \widetilde{\mathbf{C}}^{(k)} \mathbf{L}\varphi \\
& - (z - z_{k-1}) \mathbf{L}^{\mathrm{T}} \widetilde{\mathbf{C}}^{(k)} (\mathbf{L}\mathbf{u} + \overline{\boldsymbol{\varepsilon}}^{\mathrm{en}}) + \boldsymbol{\tau}_0^{(k)} + \mathbf{a}\left(z + \frac{t}{2}\right) \Bigg],
\end{aligned} \tag{63}$$

where the vector $\mathbf{a}$ and the quantities b_1 and b_2 are evaluated enforcing that the shear stress $\hat{\boldsymbol{\tau}}^{(k)}$ evaluated at the top of the laminate is zero and its integral over the thickness is equal to the resultant shear stress $\mathbf{S}$, which is obtained from the finite element analysis (cf. Eq. (62)).

As previously discussed, the proposed element is based on a linked interpolation technique, with the consideration of enhanced incompatible modes to improve the in-plane deformations. When these are assumed to be null the scheme under consideration has been rigorously proved to be robust and first-order convergent both for homogeneous plates (cf. [7]) and for anisotropic laminated ones (cf. [6]).

In the case of laminates formed by layers with orthotropic behaviour, Auricchio et al. in Ref. [6] successfully compare numerical results obtained through the adopted linked interpolation scheme (without enhanced strains) with those obtained through the well-known MITC4 plate element (cf. [9,10,12]). Furthermore, still for orthotropic layers, Ref. [2] proposes very satisfactory numerical comparisons between the enhanced linked scheme and MITC 4- and -9 node plate elements.

Accordingly, in the case of laminates formed by monoclinic layers and considering enhanced strains the proposed element is still first-order convergent and locking-free, as confirmed through the following numerical applications.

4. Numerical examples

The proposed monoclinic laminate element has been implemented in FEAP (finite element analysis program) [38] and several numerical examples are investigated in order to assess its performances. In detail, two model problems are considered, whose analytical solutions can be evaluated. In both cases, the plate mid-plane is assumed to be square $\mathscr{P} = [0,a] \times [0,a]$ and subjected to a transversal sinusoidal load: $q(x_1,x_2) = q_o \sin(\phi x_1)\sin(\phi x_2)$, with $\phi = \pi/a$. Moreover, the numerical analyses are performed assuming the shear correction factors to be constant and equal to $\chi_{11} = \chi_{22} = 5/6$, $\chi_{12} = 0$.

The error of a discrete solution is measured through the relative errors E_u, E_w and E_φ, defined as:

$$E_u^2 = \frac{\sum_{N_i}\left[(u_{h1}(N_i) - u_1(N_i))^2 + (u_{h2}(N_i) - u_2(N_i))^2\right]}{\sum_{N_i}\left[(u_1(N_i))^2 + (u_2(N_i))^2\right]}, \quad (64)$$

$$E_w^2 = \frac{\sum_{N_i}(w_h(N_i) - w(N_i))^2}{\sum_{N_i} w(N_i)^2}, \quad (65)$$

$$E_\varphi^2 = \frac{\sum_{N_i}\left[(\varphi_{h1}(N_i) - \varphi_1(N_i))^2 + (\varphi_{h2}(N_i) - \varphi_2(N_i))^2\right]}{\sum_{N_i}\left[(\varphi_1(N_i))^2 + (\varphi_2(N_i))^2\right]}, \quad (66)$$

where the sums are performed on all the nodes N_i corresponding to global interpolation parameters. Furthermore, $f(N_i)$ denotes the exact value of f at the coordinates of node N_i, while $f_h(N_i)$ is the value which is obtained by numerical computation and corresponding to a mesh parameter h. The above error measures can be also seen as discrete L^2-type errors and a h^2 convergence rate in L^2 norm actually means a h convergence rate in H^1 energy-type norm.

4.1. First validation case

In the first model problem the laminae are assumed to be orthotropic with properties corresponding to a high modulus graphite/epoxy composite, whose properties are set as follows:

$$E_L/E_T = 25, \quad \nu_{TT} = 0.25,$$
$$G_{LT}/E_T = 0.5, \quad G_{TT}/E_T = 0.2,$$

where the indexes L and T indicate the longitudinal and the transversal directions, E indicates a Young's modulus, ν a Poisson ratio, G a shear modulus.

The symmetrical 0/90/90/0 and the unsymmetrical 0/90/90 cross-ply lamination sequences are considered under the assumption of simply supported boundary conditions:

$$u_2 = 0, \quad w = 0, \quad \varphi_2 = 0 \qquad \text{at } x_1 = 0 \text{ and } x_1 = a,$$
$$u_1 = 0, \quad w = 0, \quad \varphi_1 = 0 \qquad \text{at } x_2 = 0 \text{ and } x_2 = a.$$

Following Ref. [34], the exact solution for the case under investigation has the form:

$$\begin{cases} w = \overline{w}\sin(\phi x_1)\sin(\phi x_2), \\ \varphi_1 = \overline{\varphi}_1\cos(\phi x_1)\sin(\phi x_2), \\ \varphi_2 = \overline{\varphi}_2\sin(\phi x_1)\cos(\phi x_2), \\ u_1 = \overline{u}_1\cos(\phi x_1)\sin(\phi x_2), \\ u_2 = \overline{u}_2\sin(\phi x_1)\cos(\phi x_2). \end{cases} \quad (67)$$

The amplitudes of the unknown fields can be computed considering the functional (26). In detail, performing its variation with respect to $\mathbf{S}$ and requiring a strong satisfaction of the corresponding condition, it follows that the solution $(\tilde{\mathbf{u}}, \tilde{\boldsymbol{\varphi}}, \tilde{w})$ minimizes the potential energy functional (cf. Eq. (27)):

$$\widetilde{\Pi} = \Pi^{(mb)}(\mathbf{u},\boldsymbol{\varphi}) + \frac{1}{2}\int_{\mathscr{P}} \mathbf{H}^{-1}\left(\boldsymbol{\varphi} + \overline{\nabla} w\right)\cdot\left(\boldsymbol{\varphi} + \overline{\nabla} w\right) \mathrm{d}A - \int_{\mathscr{P}} q w \,\mathrm{d}A. \quad (68)$$

Accordingly, using the positions (67) and requiring the potential energy stationarity, an algebraic system of five equations is obtained and it may be solved in terms of the five amplitudes $\overline{u}_1$, $\overline{u}_2$, $\overline{w}$, $\overline{\varphi}_1$ and $\overline{\varphi}_2$.

Due to symmetry considerations, only one quarter of the plate (i.e. $x_1 \in [0,a/2]$, $x_2 \in [0,a/2]$) is analyzed and different values of the side-to-thickness ratio $\lambda = a/t$ are considered. Moreover, the analyses are performed using regular meshes (RM) as well as distorted meshes (DM) as shown in Fig. 2.

Fig. 3 shows the relative errors (64)–(66) versus the number of nodes per side for the considered lamination sequences, with $\lambda = 10$. The results have been obtained considering regular meshes and, only in the case of E_w—in order to have more compact representations—, MEML4

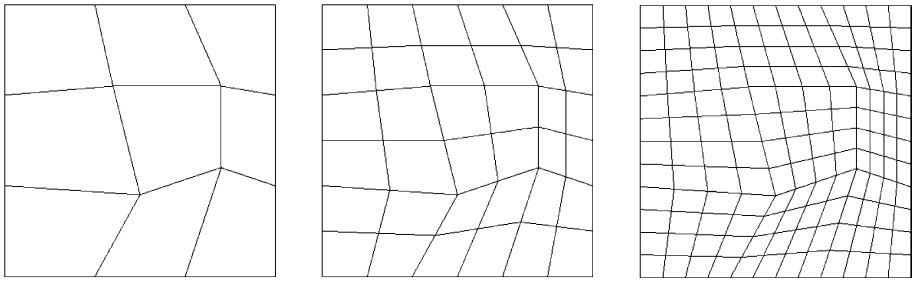


Fig. 2. 3×3, 6×6, 12×12 distorted meshes adopted for laminate computations.

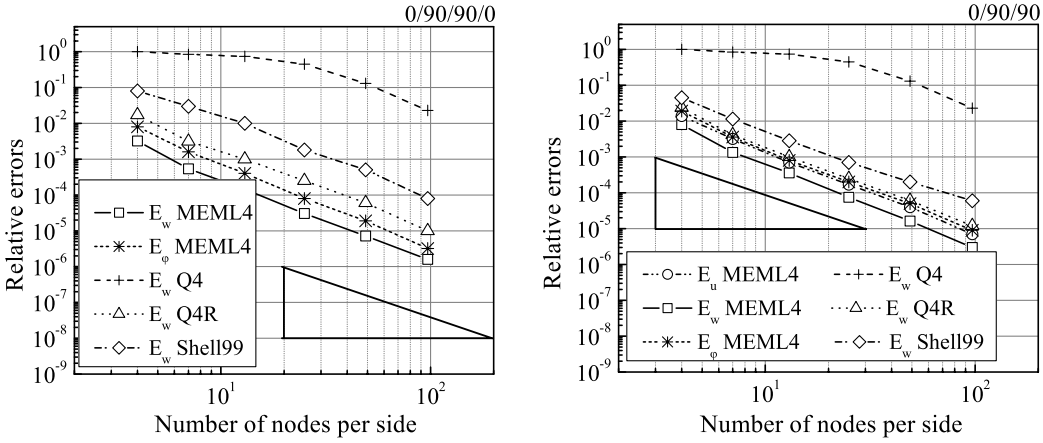


Fig. 3. Relative errors (E_w, E_φ, E_u) versus the number of nodes per side for simply supported 0/90/90/0 and 0/90/90 graphite/epoxy square laminates subjected to transversal sinusoidal load ($\lambda = 10$).

results are compared with those obtained by three different 4-node elements: Q4, Q4R and Shell99. The first two are isoparametric displacement-based elements [43]. The element Q4R is quite similar to Q4 except for the fact that a reduced numerical integration for the shear terms are adopted to avoid locking. The third one, the element Shell99, is a linear layered structural shell and it is implemented into the commercial code Ansys 7.1®. It is based on a linear displacement formulation which takes into account shear deformations through a FSDT approach. For this element the material properties of each layer may be at the most orthotropic in the plane of the element.

It is interesting observing that for both the lamination sequences a quadratic convergence rate appears both for MEML4 and for Q4R and Shell99 (in the figures the slope corresponding to the theoretical L^2 convergence rate is represented). Also the element Q4 seems to exhibit a quadratic convergence rate but, as a result of locking phenomena, this happens only when the discretization is very refined.

Fig. 4 shows the relative errors versus λ for the two lamination sequences, respectively. The results refer to regular meshes of 12×12 elements. It turns out that the element Q4 exhibits locking. On the other hand, the elements MEML4, Q4R and Shell99 are practically insensitive to the variations of λ, so that they appear to be locking free.

Thus, it can be stated that MEML4 exhibits a better accuracy and appears to be fully robust and reliable.

Table 1 reports the dimensionless displacement $w^* = wE_T/(q_o a)$ at the plate center and the rotation $\varphi^* = \varphi_1 E_T/q_o$ at $x_1 = 0$, $x_2 = a/2$ for symmetrical 0/90/90/0 cross-ply laminates, with $\lambda = 10$.

Table 2 reports w^* and φ^*, previously defined, and the dimensionless horizontal displacement $u^* = u_1 E_T/(q_o a)$ at $x_1 = 0$, $x_2 = a/2$ for unsymmetrical 0/90/90 laminates, with $\lambda = 10$.

The accuracy and the convergence of the numerical solutions of the element MEML4 are once more evident. Moreover, it can be emphasized that both in-plane and out-of-plane displacements are in good agreement with the analytical solutions (AS), even with coarse or distorted meshes.

Furthermore, the ability of the element MEML4 to compute satisfactory interlaminar stresses has been investigated. Figs. 5–8 show the dimensionless shear stress

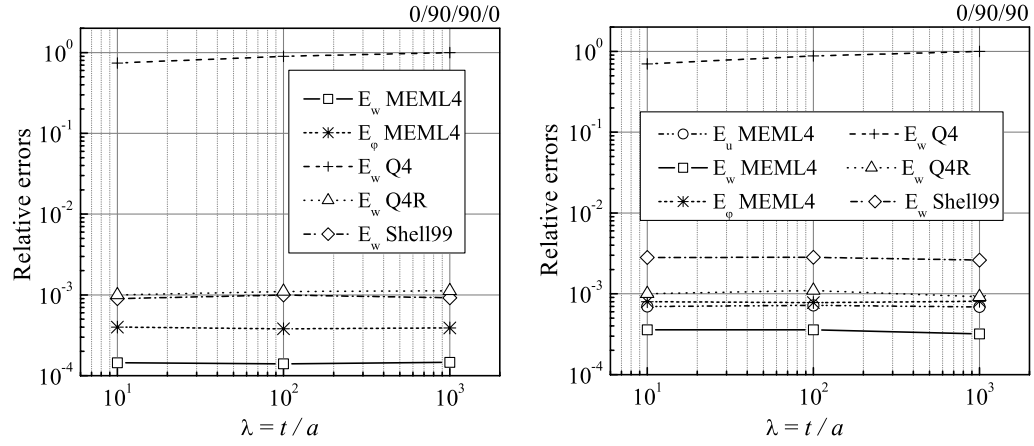


Fig. 4. Relative errors (E_w, E_φ, E_u) versus λ for simply supported 0/90/90/0 and 0/90/90 graphite/epoxy square laminates subjected to transversal sinusoidal load (12×12 square MEML4 elements).

Table 1
Transversal displacement w^* and rotation φ^* for simply supported 0/90/90/0 graphite/epoxy square laminates subjected to transversal sinusoidal load: comparison between analytical and finite-element solutions

Mesh		3×3		6×6		12×12	
		(RM)	(DM)	(RM)	(DM)	(RM)	(DM)
MEML4	w^*	6.6381	6.5231	6.6302	6.6168	6.6279	6.6258
	φ^*	−12.4306	−12.3053	−12.4745	−12.4655	−12.4853	−12.4831
Shell99	w^*	6.3292	6.0134	6.5521	6.4923	6.6082	6.6025
	φ^*	−11.9281	−11.2177	−12.3480	−12.2916	−12.4540	−12.4412
Q4R	w^*	6.5853	6.4532	6.6172	6.5972	6.6233	6.6215
	φ^*	−12.2867	−11.4177	−12.4303	−12.4016	−12.4791	−12.4782
(AS)		$w^* = 6.6271$				$\varphi^* = -12.4898$	

Table 2
Transversal displacement w^*, rotation φ^* and horizontal displacement u^* for simply supported 0/90/90 graphite/epoxy square laminates subjected to transversal sinusoidal load: comparison between analytical and finite-element solutions

Mesh		3×3		6×6		12×12	
		(RM)	(DM)	(RM)	(DM)	(RM)	(DM)
MEML4	w^*	10.7109	10.2324	10.7067	10.6998	10.755	10.7048
	φ^*	−29.3389	−29.1365	−29.3754	−29.3648	−29.3868	−29.3862
	u^*	−0.8799	−0.9192	−0.8654	−0.8686	−0.8619	−0.8621
Shell99	w^*	10.2231	9.4592	10.5832	10.5114	10.6752	10.6663
	φ^*	−28.0671	−25.0231	−29.0543	−28.8269	−29.3052	−29.2981
	u^*	−0.8220	−0.7333	−0.8509	−0.8459	−0.8583	−0.8568
Q4R	w^*	10.6446	10.0458	10.6948	10.6732	10.7035	10.7023
	φ^*	−29.5324	−28.8956	−29.4147	−29.4365	−29.3841	−29.3821
	u^*	−0.8991	−0.9625	−0.8683	−0.8728	−0.8627	−0.8631
(AS)		$w^* = 10.7052$		$\varphi^* = -29.3889$		$u^* = -0.8607$	

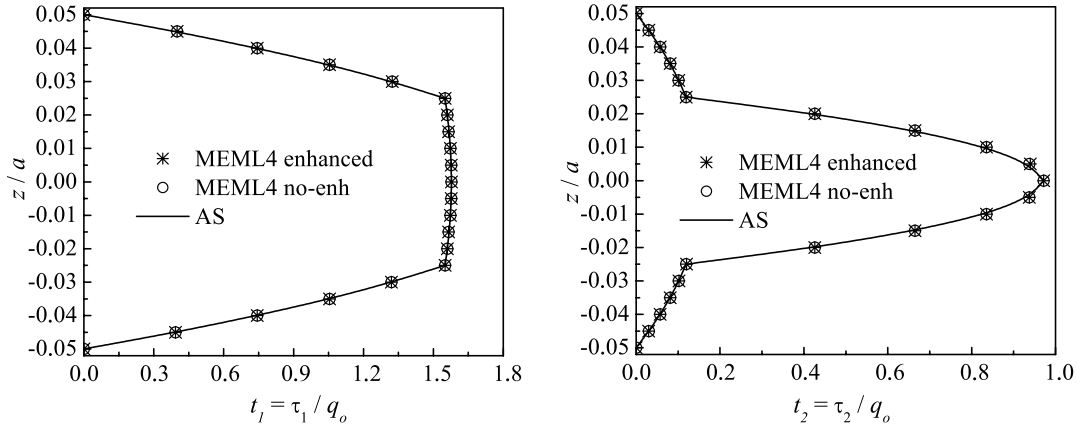


Fig. 5. Shear stress profiles $t_1 = \sigma_{13}/q_o$ and $t_2 = \sigma_{23}/q_o$ at $x_1 = x_2 = a/4$ for simply supported 0/90/90/0 graphite/epoxy square laminates subjected to transversal sinusoidal load. Comparison between numerical and analytical solutions.

profiles $t_\alpha = \tau_\alpha/q_o = \sigma_{\alpha 3}/q_o$ and the normal stress ones $s_{\alpha\alpha} = \sigma_{\alpha\alpha}/q_o$ evaluated at $x_1 = x_2 = a/4$ for 0/90/90/0 and 0/90/90 laminates, with $\lambda = 10$. The results refer to regular meshes of 5×5 MEML4 elements and they are compared with the analytical solutions. For the shear stress profiles, results obtained with and without the enhanced strains are presented. It is worth observing that, in the case of symmetrical lamination sequences, no differences exist between the enhanced and non-enhanced solutions, because the transversal loading does not induce horizontal deformations. As a consequence, the enhanced modes are not active for this problem. On the other hand, in the case of unsymmetrical laminates there is a significant improvement between the enhanced and non-enhanced solutions. In fact, the transversal loading induce horizontal deformations in 0/90/90 unsymmetrical laminates. Accordingly, the enhanced modes are now active and they produce an evident improvement of the numerical solutions.

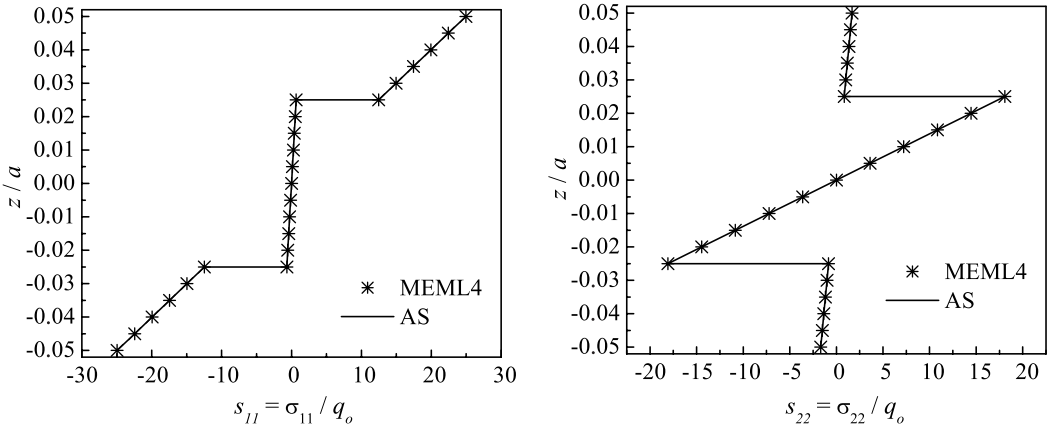


Fig. 6. Normal stress profiles $s_{11} = \sigma_{11}/q_o$ and $s_{22} = \sigma_{22}/q_o$ at $x_1 = x_2 = a/4$ for simply supported 0/90/90/0 graphite/epoxy square laminates subjected to transversal sinusoidal load. Comparison between numerical and analytical solutions.

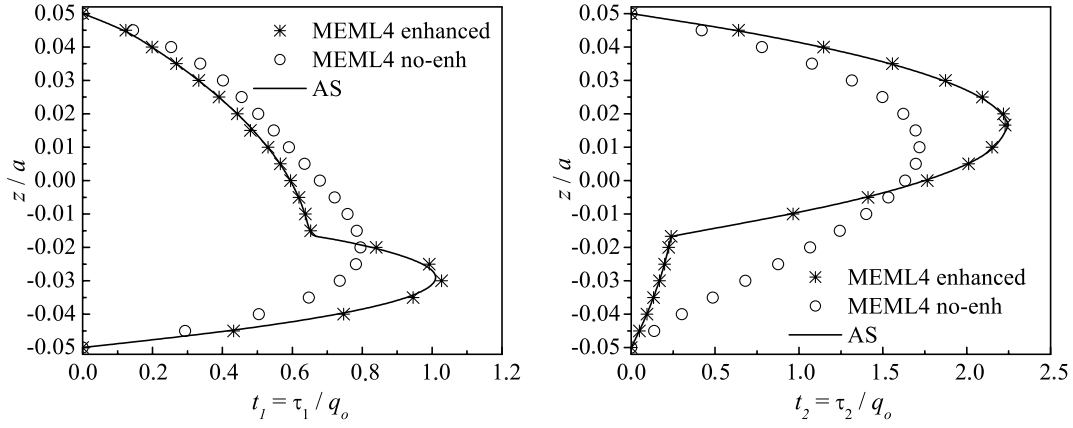


Fig. 7. Shear stress profiles $t_1 = \sigma_{13}/q_o$ and $t_2 = \sigma_{23}/q_o$ at $x_1 = x_2 = a/4$ for simply supported 0/90/90 graphite/epoxy square laminates subjected to transversal sinusoidal load. Comparison between numerical and analytical solutions.

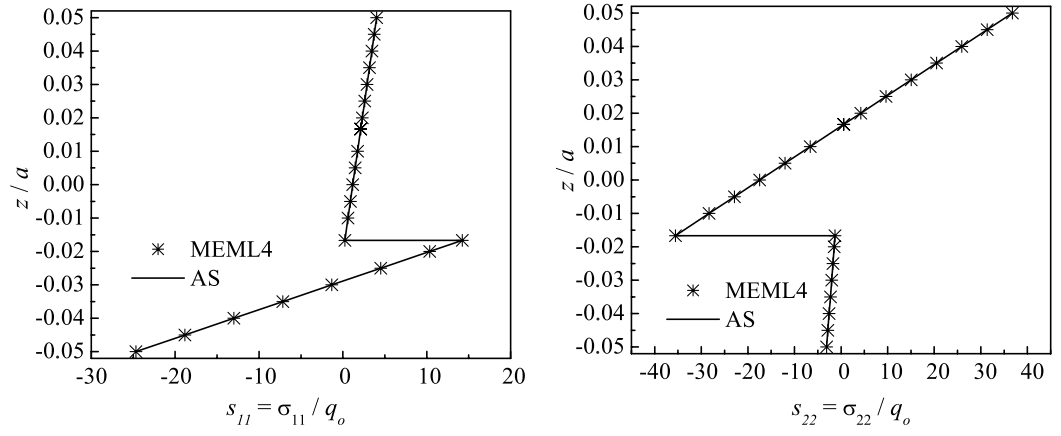


Fig. 8. Normal stress profiles $s_{11} = \sigma_{11}/q_o$ and $s_{22} = \sigma_{22}/q_o$ at $x_1 = x_2 = a/4$ for simply supported 0/90/90 graphite/epoxy square laminates subjected to transversal sinusoidal load. Comparison between numerical and analytical solutions.

4.2. Second validation case

Here, the laminated plates are assumed to be formed by layers with monoclinic material symmetry. In detail, two different types of laminae are considered. The first one is constituted by potassium tartrate (DKT), whereas the second by ethylene diamine tartrate (EDT). These materials are generally employed for realizing laminae used in piezoelectric applications. Table 3 reports apiece the 13 independent elastic constants evaluated at constant electric field.

Table 3
Elastic moduli for piezoelectric materials evaluated at constant electric field (GPa)

	$\mathscr{C}_{1111}$	$\mathscr{C}_{1122}$	$\mathscr{C}_{1133}$	$\mathscr{C}_{1112}$	$\mathscr{C}_{2222}$	$\mathscr{C}_{2233}$	$\mathscr{C}_{2212}$
DKT	27.72	10.14	14.98	2.35	51.32	12.38	6.95
EDT	64.18	26.84	13.10	−13.16	22.57	10.30	−7.38
	$\mathscr{C}_{3333}$	$\mathscr{C}_{3312}$	$\mathscr{C}_{2323}$	$\mathscr{C}_{2313}$	$\mathscr{C}_{1313}$	$\mathscr{C}_{1212}$	
DKT	37.93	−0.16	8.85	0.48	8.18	11.57	
EDT	33.58	0.06	5.22	0.10	5.23	11.64	

The symmetrical DKT/EDT/DKT and the unsymmetrical EDT/DKT laminates are analyzed. In the case of the previously defined transversal sinusoidal load, the analytical FSDT closed-form solution can be expressed as:

$$\begin{cases} w = \overline{w}\sin(\phi x_1)\sin(\phi x_2) + \widetilde{w}\cos(\phi x_1)\cos(\phi x_2), \\ \varphi_1 = \overline{\varphi}_1\cos(\phi x_1)\sin(\phi x_2) + \widetilde{\varphi}_1\sin(\phi x_1)\cos(\phi x_2), \\ \varphi_2 = \overline{\varphi}_2\sin(\phi x_1)\cos(\phi x_2) + \widetilde{\varphi}_2\cos(\phi x_1)\sin(\phi x_2), \\ u_1 = \overline{u}_1\cos(\phi x_1)\sin(\phi x_2) + \widetilde{u}_1\sin(\phi x_1)\cos(\phi x_2), \\ u_2 = \overline{u}_2\sin(\phi x_1)\cos(\phi x_2) + \widetilde{u}_2\cos(\phi x_1)\sin(\phi x_2), \end{cases} \tag{69}$$

where the amplitudes $(\bar{\cdot})$ and $(\tilde{\cdot})$ of the unknown fields are computed by solving the algebraic system obtained using positions (69) and requiring the stationarity for the functional (68). It is worth observing that, as a consequence of the positions (69), the solution is referred to non-homogeneous boundary conditions on the plate's edges. Moreover, since under these conditions numerical solutions are not expected to be symmetric in the plane of the plate, the laminates are entirely discretized using meshes based on MEML4 elements. Regular meshes as well as distorted meshes are employed.

For the two considered lamination sequences and with reference to regular meshes, Fig. 9 shows the relative errors versus the number of nodes per side (with $\lambda = 10$) and versus the side-to-thickness ratio (24×24 MEML4 elements). Again, the element appears to be locking free and it exhibits a quadratic convergence rate.

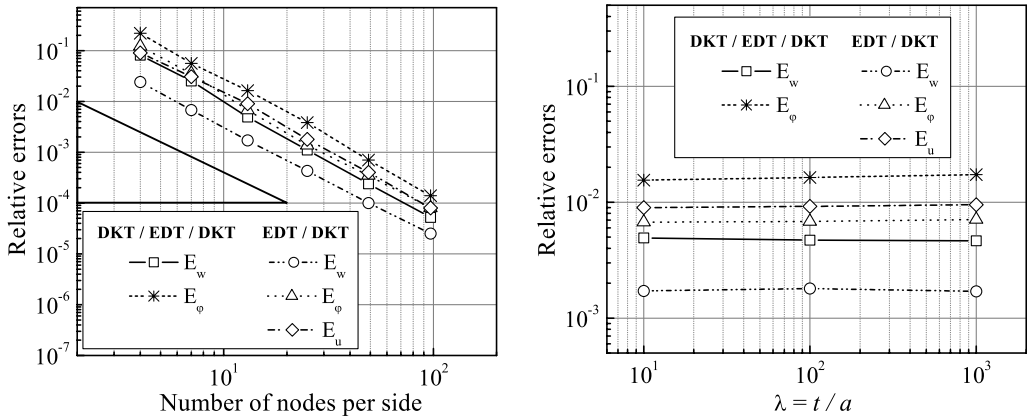


Fig. 9. Relative errors (E_w, E_φ, E_u) versus: the number of nodes per side ($\lambda = 10$); the side-to-thickness ratio λ (24×24 square MEML4 elements). DKT/EDT/DKT and EDT/DKT square laminates subjected to transversal sinusoidal load.

Table 4
Dimensionless displacements w^*, φ^* and u^* for DKT/EDT/DKT and EDT/DKT square laminates subjected to transversal sinusoidal load: comparison between analytical and finite-element solutions

Mesh		3×3		6×6		12×12	
		(RM)	(DM)	(RM)	(DM)	(RM)	(DM)
DKT/EDT/DKT	w^*	1.0918	0.9667	1.1145	1.1095	1.1189	1.1184
	φ^*	−3.4837	−4.3175	−3.3517	−3.3903	−3.3106	−3.2823
(AS)			$w^* = 1.1200$			$\varphi^* = -3.2980$	
EDT/DKT	w^*	1.1583	1.0112	1.1642	1.1605	1.1657	1.1654
	φ^*	−3.4706	−3.9758	−3.3750	−3.3911	−3.3478	−3.3457
	u^*	−0.0539	−0.0491	−0.0551	−0.0549	−0.0555	−0.0555
(AS)			$w^* = 1.1661$		$\varphi^* = -3.3524$		$u^* = -0.0556$

Table 4 reports the numerical solutions for the dimensionless transversal displacement $w^* = w/a$ at the plate center, the rotation $\varphi^* = \varphi_1$ and the dimensionless horizontal displacement $u^* = u_1/a$ at $x_1 = 0$, $x_2 = a/2$ for DKT/EDT/DKT ($u^* = 0$) and EDT/DKT laminates, in the case of $\lambda = 10$ and $q_o = 1$ GPa.

Finally, Figs. 10–13 show the dimensionless shear stress profiles t_α and the normal stress ones $s_{\alpha\alpha}$ evaluated at

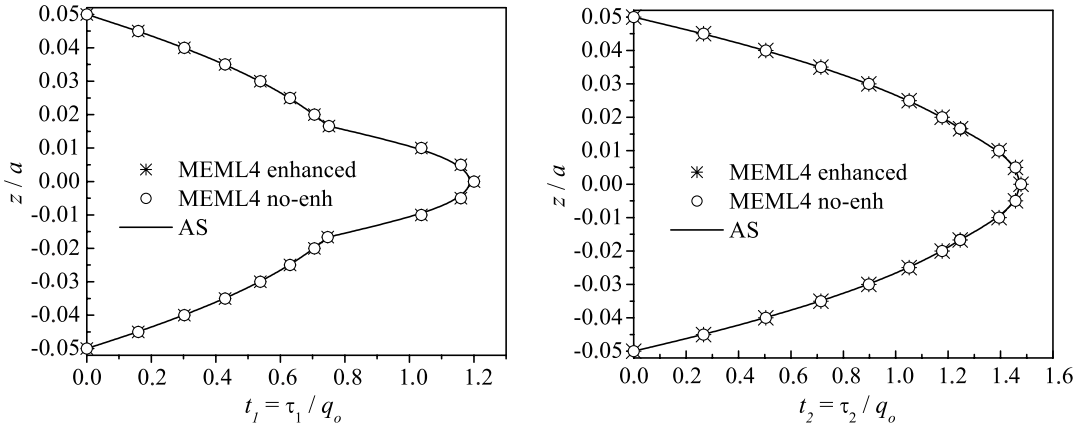


Fig. 10. Dimensionless shear stress profiles $t_1 = \sigma_{13}/q_o$ and $t_2 = \sigma_{23}/q_o$ at $x_1 = x_2 = a/4$ for DKT/EDT/DKT square laminates subjected to transversal sinusoidal load. Comparison between numerical and analytical solutions.

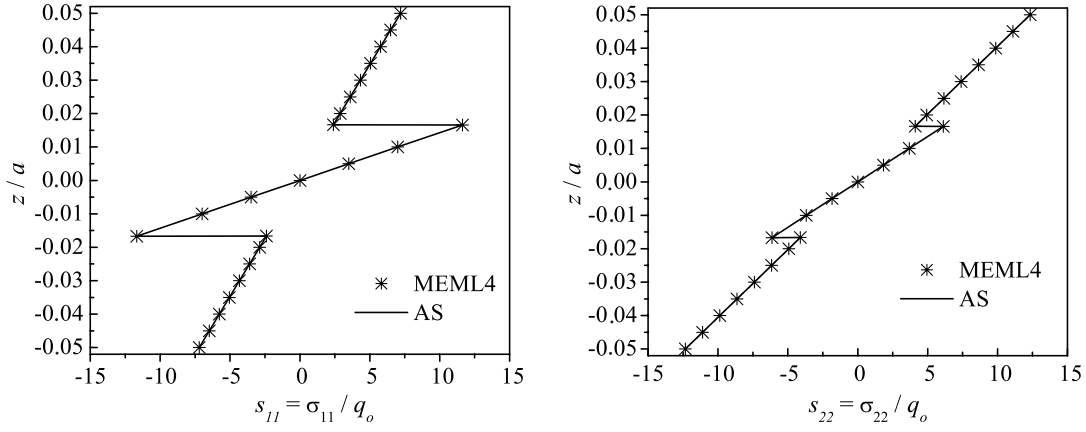


Fig. 11. Dimensionless normal stress profiles $s_{11} = \sigma_{11}/q_o$ and $s_{22} = \sigma_{22}/q_o$ at $x_1 = x_2 = a/4$ for DKT/EDT/DKT square laminates subjected to transversal sinusoidal load. Comparison between numerical and analytical solutions.

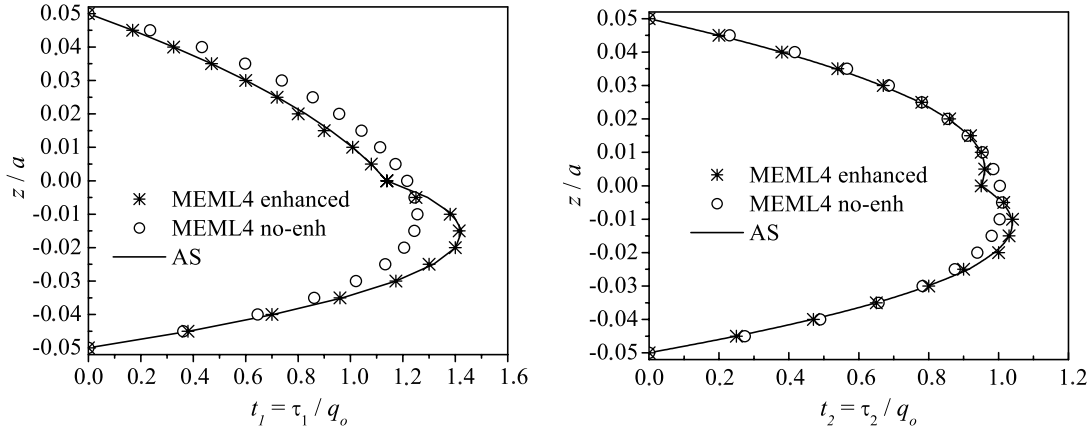


Fig. 12. Dimensionless shear stress profiles $t_1 = \sigma_{13}/q_o$ and $t_2 = \sigma_{23}/q_o$ at $x_1 = x_2 = a/4$ for EDT/DKT square laminates subjected to transversal sinusoidal load. Comparison between numerical and analytical solutions.

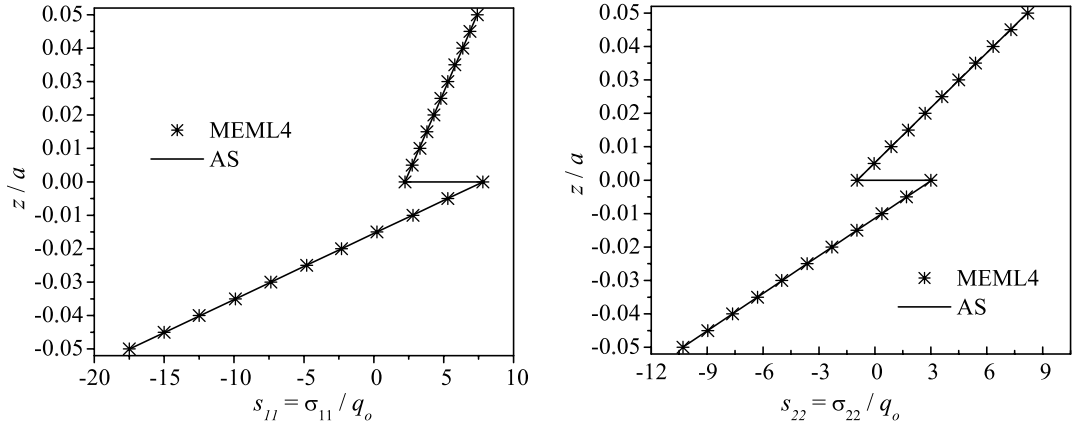


Fig. 13. Dimensionless normal stress profiles $s_{11} = \sigma_{11}/q_o$ and $s_{22} = \sigma_{22}/q_o$ at $x_1 = x_2 = a/4$ for EDT/DKT square laminates subjected to transversal sinusoidal load. Comparison between numerical and analytical solutions.

$x_1 = x_2 = a/4$ and in the case of numerical analyses based on regular meshes of 10×10 MEML4 elements. The numerical results are compared with the corresponding analytical solutions (AS).

As in the previously discussed validation case, the improvement between the enhanced and non-enhanced shear stress profiles can be appreciated in the case of unsymmetrical laminates. Accordingly, the interlaminar stresses computed by MEML4 are in good agreement with respect to the analytical solutions.

5. Concluding remarks

A partial mixed-enhanced finite-element formulation for the analysis of composite laminated plates formed by layers with monoclinic constitutive behaviour is presented. Starting from first-order shear deformation theory, the formulation includes as primary variables the resultant shear stresses and, in order to improve the in-plane deformations, enhanced incompatible modes. Accordingly, a 4-node finite element is developed and is a generalization of the element proposed in [5] to the case of monoclinic layers. The element is obtained through a linked interpolation scheme (cf. [3]), involving bubble functions for the rotation degrees of freedom and linking functions between rotations and transversal displacements. The solvability of the variational formulation has been proved whereas effectiveness and convergence of the proposed finite element have been confirmed through several numerical applications using cross-ply laminated plates as well as laminates formed by layers with monoclinic constitutive symmetry, such as those used in piezoelectric applications. The comparisons with both available numerical and analytical solutions highlight that the element shows a h^2 convergence rate in L^2 and it does not suffer from shear locking phenomena. The proposed numerical examples show that the element provides very accurate in-plane and out-of-plane displacements. Furthermore, a technique for the recovery of transversal shear stress profiles, which is based on three-dimensional equilibrium equations, is adopted. As the specialistic literature confirms (e.g. [2,4,20]), this approach leads to shear stress profiles in good agreement with the 3D ones. Therefore, it can be emphasized that even coarse or distorted meshes produce accurate results, not only in terms of in-plane/out-of-plane displacements but also in terms of interlaminar shear and normal stresses, for both symmetrical and unsymmetrical laminated plates formed by layers having at least a monoclinic symmetry. Accordingly, the proposed finite element opens the possibility of interesting works related to the modelling and analysis of the activation and development of delamination mechanisms in monoclinic laminates.

Acknowledgements

This research was developed within the framework of Lagrange Laboratory, an European research group between CNRS, CNR, University of Rome "Tor Vergata", University of Montpellier II, ENPC and LCPC.

References

[1] Aitharaju VR, Averill RC. C^0 zig-zag kinematic displacement models for the analysis of laminated composites. Mech Comp Mater Struct 2000;6:31–56.
[2] Alfano G, Auricchio F, Rosati L, Sacco E. MITC finite elements for laminated composite plates. Int J Numer Meth Eng 2001;50:707–38.
[3] Auricchio F, Taylor RL. A shear deformable plate element with an exact thin limit. Comput Meth Appl Mech Eng 1994;118:393–412.
[4] Auricchio F, Sacco E. Partial-mixed formulation and refined models for the analysis of composite laminates within an FSDT. Compos Struct 1999;46:103–13.
[5] Auricchio F, Sacco E. A mixed-enhanced finite-element for the analysis of laminated composite plates. Int J Numer Meth Eng 1999;44:1481–504.
[6] Auricchio F, Lovadina C, Sacco E. Analysis of mixed finite elements for laminated composite plates. Comput Meth Appl Mech Eng 2001;190:4767–83.
[7] Auricchio F, Lovadina C. Analysis of kinematic linked interpolation methods for Reissner–Mindlin plate problems. Comput Meth Appl Mech Eng 2001;19:2465–82.
[8] Auricchio F, Sacco E, Vairo G. A mixed FSDT finite-element formulation for the analysis of composite laminates without shear

correction factors. Mechanical modelling and computational issues in civil engineering. Lecture notes in appl and comput mech, vol. 23. Berlin: Springer-Verlag. p. 345–58.
[9] Bathe KJ, Brezzi F. On the convergence of a four-node plate bending element based on Mindlin–Reissner plate theory and a mixed interpolation. In: Whiteman JR, editor. MAFELAP V, London, 1985. p. 491–503.
[10] Bathe KJ, Bucalem MJ, Brezzi F. Displacement and stress convergence of MITC plate bending elements. Eng Comput 1990;7:291–302.
[11] Bathe KJ. Finite element procedures. Englewood Cliffs: Prentice-Hall; 1995.
[12] Bathe KJ. The inf–sup condition and its evaluation for mixed finite element methods. Comput Struct 2001;79:243–52.
[13] Bisegna P, Sacco E. A layer-wise laminate theory rationally deduced from three-dimensional elasticity. J Appl Mech 1997;64:538–44.
[14] Bisegna P, Sacco E. A rational deduction of plate theories from the three-dimensional linear elasticity. Z Angew Math Mech 1997;77:349–66.
[15] Braess D. Enhanced assumed strain elements and locking in membrane problems. Comput Meth Appl Mech Eng 1998;165:155–74.
[16] Brezzi F, Fortin M. Mixed and hybrid finite element methods. Berlin: Springer-Verlag; 1991.
[17] Brezzi F, Fortin M, Stenberg R. Error analysis of mixed-interpolated elements for Reissner–Mindlin plates. Math Models Meth Appl Sci 1991;1:125–51.
[18] Carrera E. C_z^0-requirements: models for two-dimensional analysis of multilayered structures. Compos Struct 1997;37:373–84.
[19] Carrera E. Single-layer vs multi-layers plate modelings on the basis of Reissner's mixed theorem. Am Inst Aeron Astron J 2000;38: 342–3.
[20] Carrera E. A priori vs. a posteriori evaluation of transverse stresses in multilayered orthotropic plates. Compos Struct 2000;48:245–60.
[21] Fares ME. Non-linear analysis of composite laminated plates using a refined first-order theory. Compos Struct 1999;46:257–66.
[22] Hassis H. A high-order theory for static dynamic analysis of laminated plates using a special warping model. Euro J Mech A/ Solids 2002;21:323–32.
[23] Hughes TJR. The finite element method: linear static and dynamic finite element analysis. New York: Dover Publications; 2000.
[24] Idlbi A, Karama M, Touratier M. Comparison of various laminated plate theories. Compos Struct 1997;37:173–84.
[25] Laitinen M, Lahtinen H, Sjölind SG. Transverse shear correction factors for laminates in cylindrical bending. Commun Numer Meth Eng 1995;11:41–7.
[26] Lo KH, Christensen RM, Wu EM. A high-order theory of plate deformation. Part II: Laminated plates. J Appl Mech 1978;44:669–76.
[27] Lovadina C. Analysis of a mixed finite element method for Reissner–Mindlin plate problems. Comput Meth Appl Mech Eng 1998;163:71–85.
[28] Lovadina C, Auricchio F. On the enhanced strain technique for elasticity problems. Comput Struct 2003;81:777–87.
[29] Mindlin RD. Influence of rotatory inertia and shear on flexural motions of isotropic, elastic plates. J Appl Mech 1951;38:31–8.
[30] Noor AK, Burton WS, Peters JM. Predictor–corrector procedures for stress and free vibration analyses of multilayered composite plates and shells. Int J Comput Meth Appl Mech Eng 1990;82:341–63.
[31] Oden JT, Reddy JN. Variational methods in theoretical mechanics. Berlin: Springer-Verlag; 1976.
[32] Pai PF. A new look at the shear correction factors and warping functions of anisotropic laminates. Int J Solids Struct 1995;32:2295–313.
[33] Rao MK, Desai YM. Analytical solutions for vibrations of laminated and sandwich plates using mixed theory. Compos Struct 2004;63:361–73.
[34] Reddy JN. Mechanics of laminated composite plates, theory and analysis. Boca Raton: CRC Press; 1997.
[35] Reissner E. The effect of transverse shear deformation on the bending of elastic plates. J Appl Mech 1945;12:69–77.
[36] Simo JC, Rifai MS. A class of mixed assumed strain methods and the method of incompatible modes. Int J Numer Meth Eng 1990;29:1595–638.
[37] Taylor RL, Auricchio F. Linked interpolation for Reissner–Mindlin plate elements: Part II—A simple triangle. Int J Numer Meth Eng 1993;36:3057–66.
[38] Taylor RL. A finite-element analysis program. Technical report, Univ. of California at Berkeley, 2000.
[39] Wang CM, Reddy JN, Lee KH. Shear deformable beams and plates. Relationships with classical solutions. Oxford: Elsevier Science Ltd; 2000.
[40] Whitney JM, Pagano NJ. Shear deformation in heterogeneous anisotropic plates. J Appl Mech, Trans ASME 1970;37(92/E):1031–6.
[41] Yang PC, Norris CH, Stavsky Y. Elastic wave propagation in heterogeneous plates. Int J Solids Struct 1966;2:665–84.
[42] Zienkiewicz OC, Xu Z, Zeng LF, Samuelsson A, Wiberg NE. Linked interpolation for Reissner–Mindlin plate elements: Part I—A simple quadrilateral. Int J Numer Meth Eng 1993;36:3043–56.
[43] Zienkiewicz OC, Taylor RL. The finite element method, vol. 1. 4th ed. New York: McGraw-Hill; 1997.